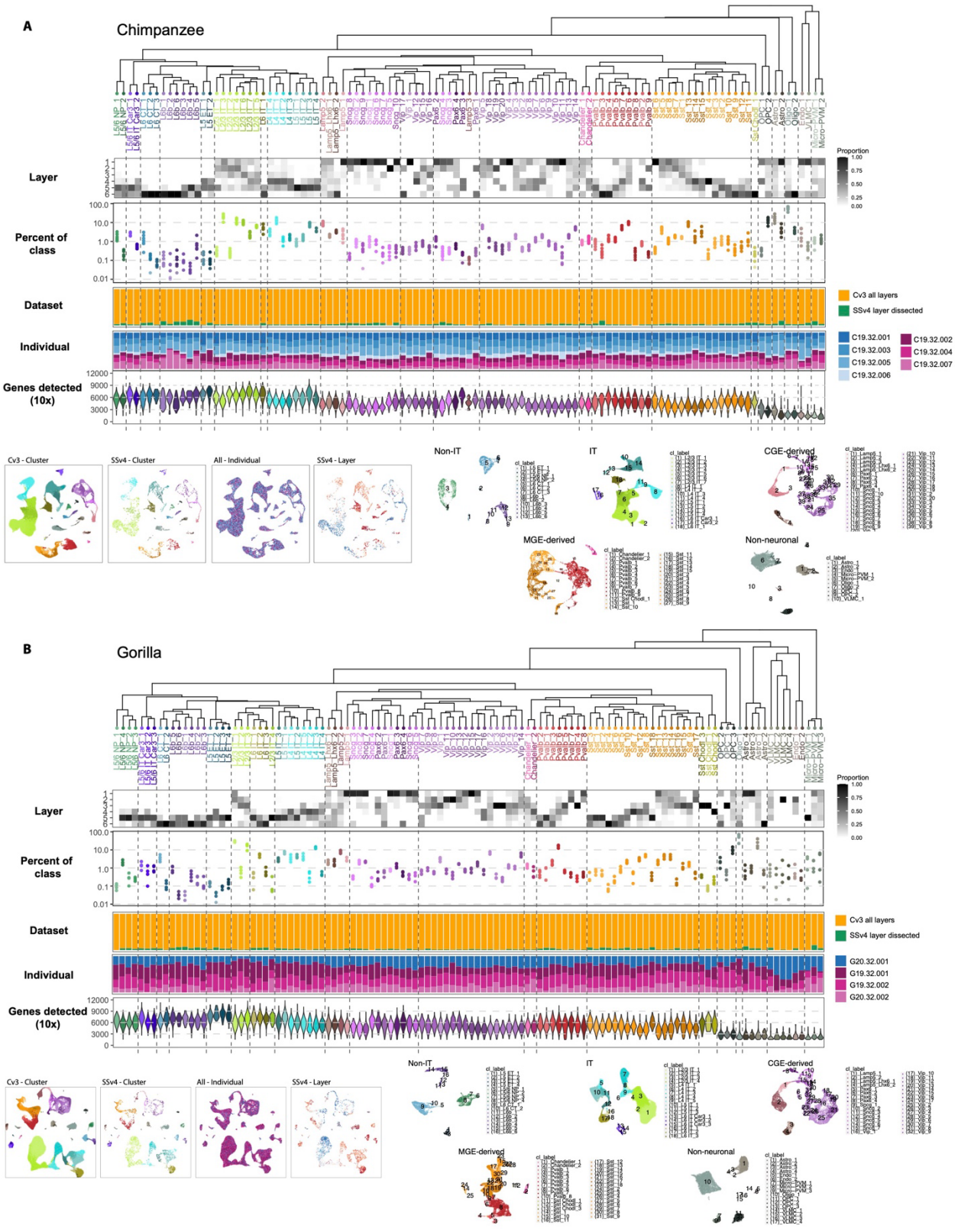

Fig. S1.
Chimpanzee and gorilla MTG taxonomies. (A, B) Dendrogram of chimpanzee **(A)** and gorilla **(B)** cell types with estimated layer distributions, cell type frequencies as a proportion of cell

class, dataset composition, individual ID, and distribution of genes detected. UMAPs of single nuclei colored by cluster, individual ID, and layer dissection.

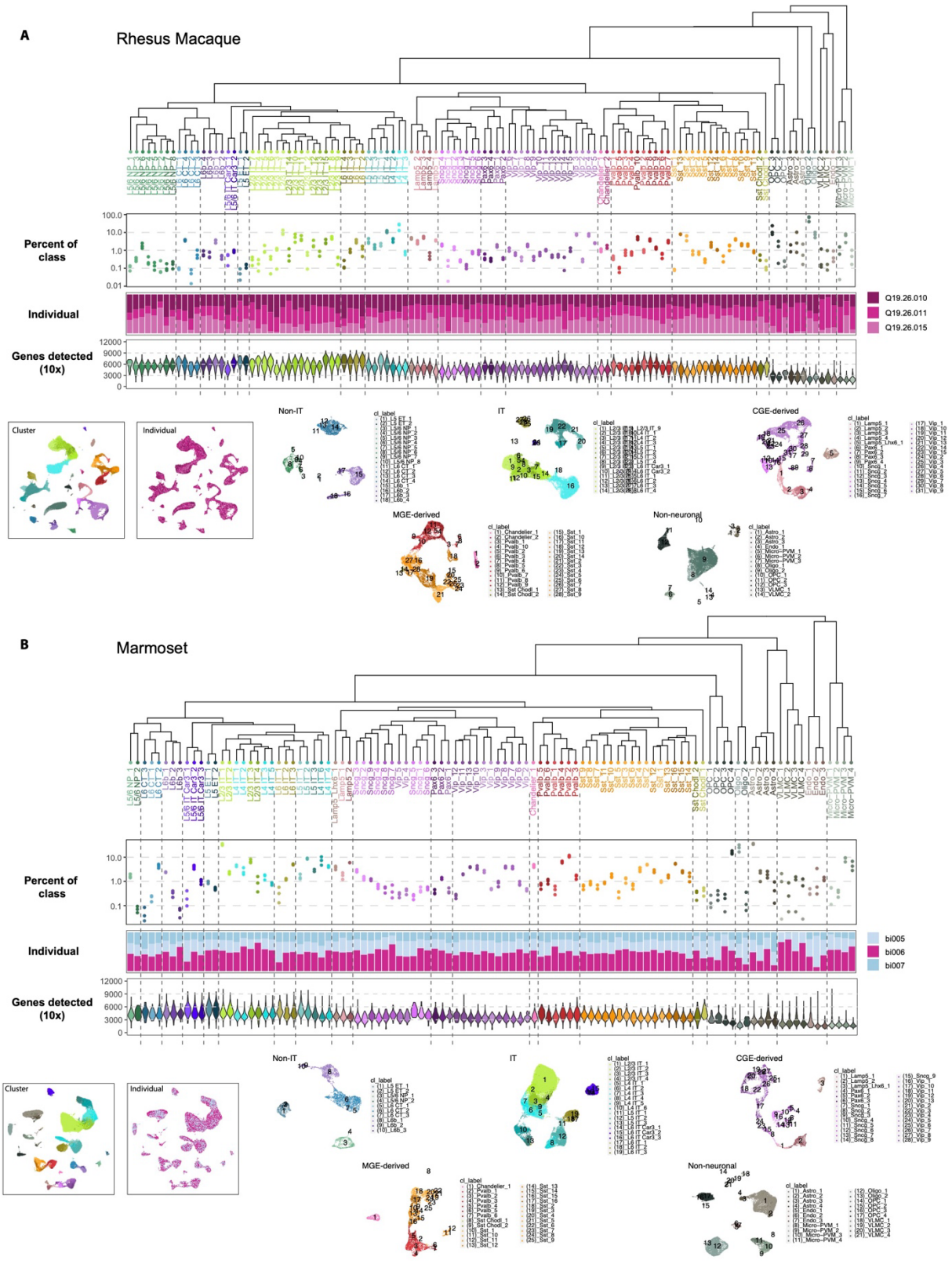

Fig. S2.

Rhesus macaque and marmoset MTG taxonomies. (A, B) Dendrogram of rhesus macaque **(A)** and marmoset **(B)** cell types with estimated layer distributions, cell type frequencies as a

proportion of cell class, dataset composition, individual ID, and distribution of genes detected. UMAPs of single nuclei colored by cluster, individual ID, and layer dissection.

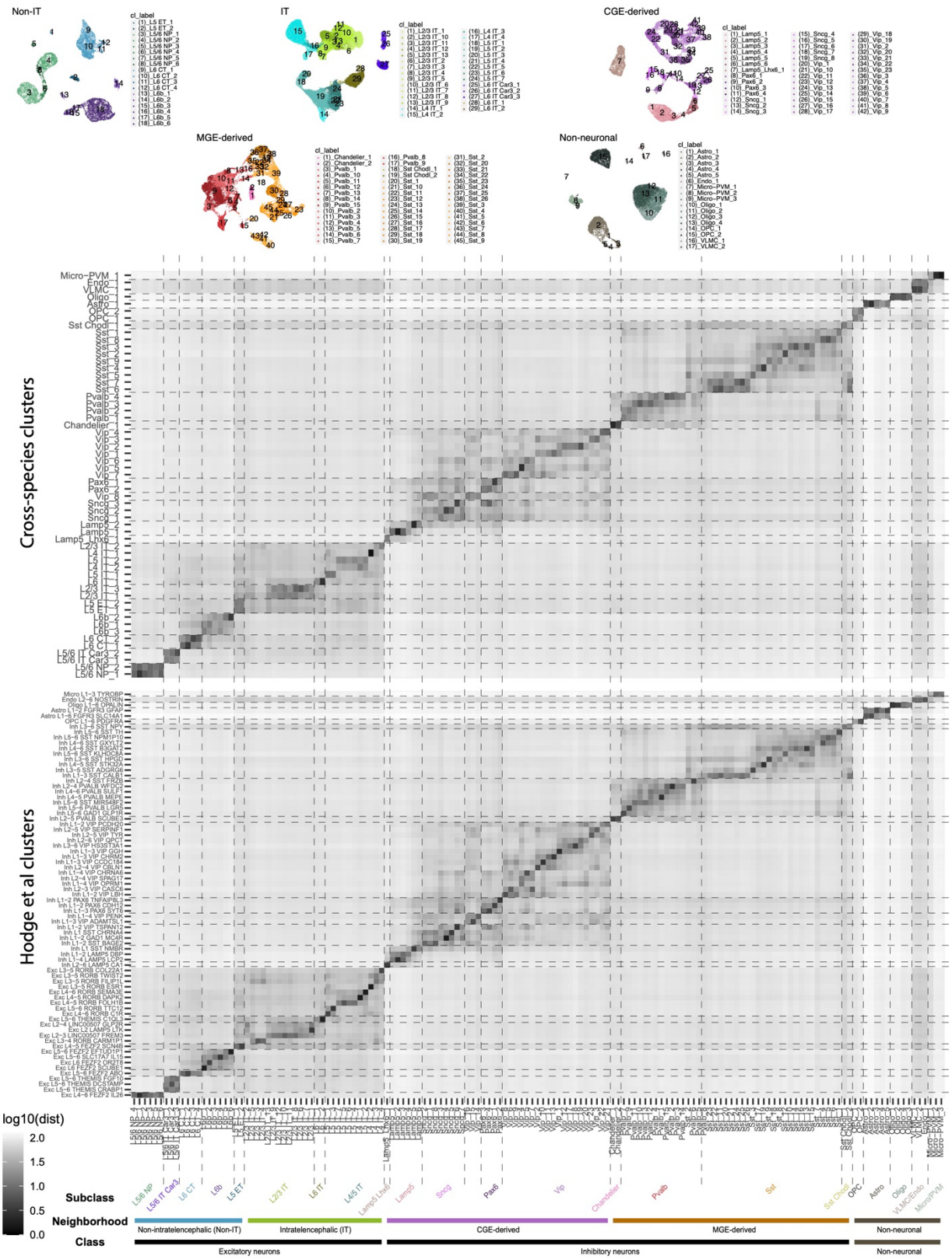

Fig. S3.

Comparison of human MTG cell types to other taxonomies. For each cell neighborhood, a UMAP of single nuclei colored by cluster. Heatmaps of log-transformed Euclidean distance

between cluster centroids of human MTG cell types (columns) and primate consensus types (top) and our previously published MTG taxonomy (bottom; (*17*)). Cell subclasses, neighborhoods, and classes are labeled at the bottom.

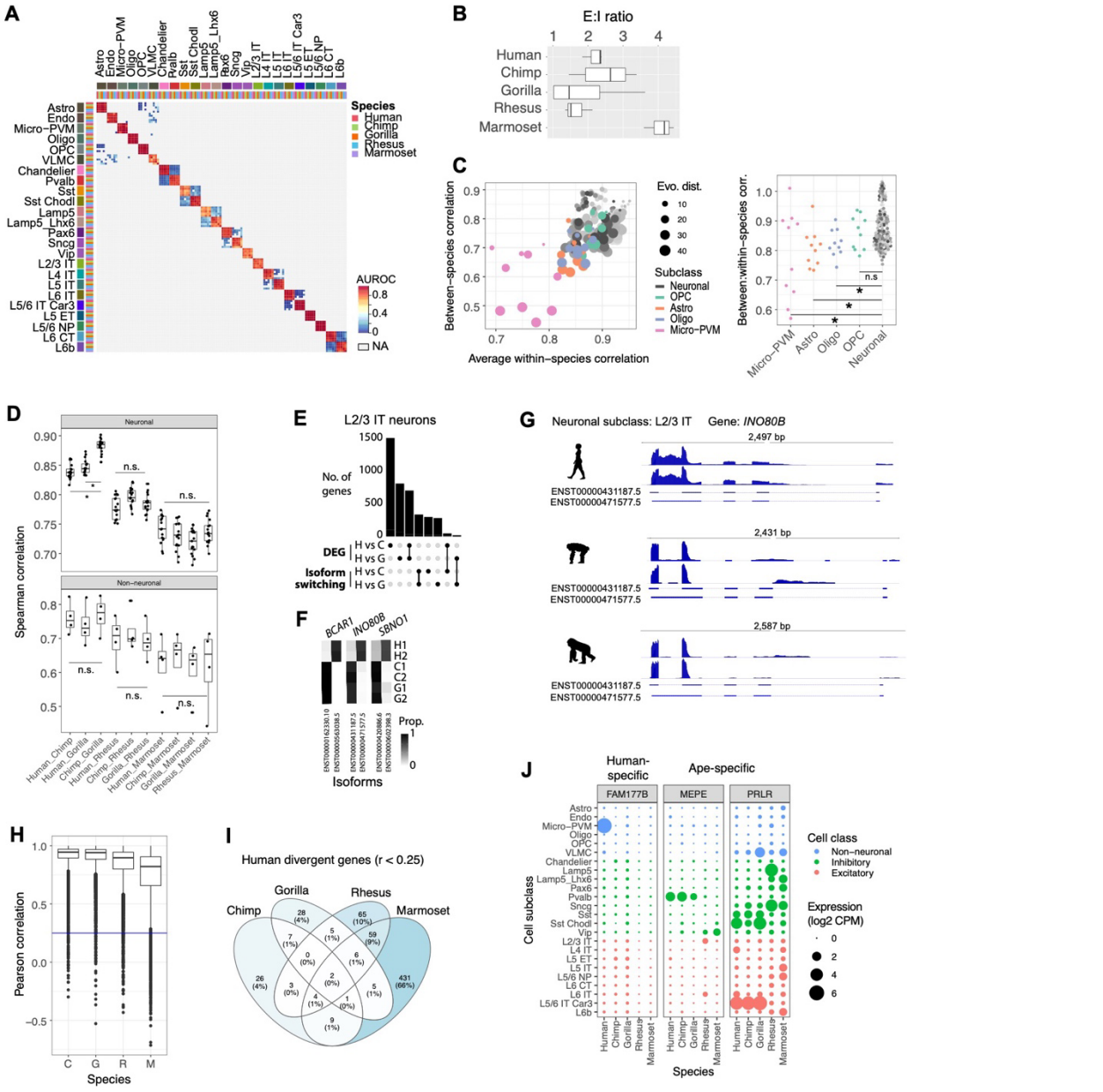

Fig. S4.

Cell subclass comparisons across species. (A) Heatmap of 1-vs-best MetaNeighbor scores for cell subclasses. Each column shows the performance for a single training group across the three test datasets. AUROCs are computed between the two closest neighbors in the test dataset, where the closer neighbor will have the higher score, and all others are shown in gray (NA). Dark red 3x3 blocks along the diagonal indicate high transcriptomic similarity across all five species. **(B)** Boxplots of the estimated ratio of excitatory to inhibitory neurons across individuals of each species based on snRNA-seq sampling. **(C)** Left: Comparison of cell subclass similarity (expression correlation) within and between species. Each point represents a pairwise species comparison where the point color indicates subclass and size indicates the evolutionary distance to the most recent common ancestor. Within-species similarity was calculated as the average of the average interindividual correlations for the two species being compared. Right: Bee swarm plots showing the ratio of between-species to average within-species correlations for all pairs of

species and grouped by non-neuronal subclasses and neurons. The correlation ratio of non-neuronal subclasses was compared to the neuronal ratio using one-sided t tests with Holm-Bonferroni p-value correction for multiple testing (* $P < 0.05$). **(D)** Comparison of expression correlations of neuronal and non-neuronal subclasses across pairs of species. ANOVA tests were used to test for significant differences in correlations across great apes, between great apes and rhesus, and between great apes and marmoset. A post-hoc Tukey HSD test between pairs of great apes showed that chimpanzee and gorilla were significantly more highly correlated than human and chimpanzee or human and gorilla (* $P < 0.05$). **(E)** Upset plot of intersections of DEGs and genes with differential isoform usage in L2/3 IT neurons between humans and chimpanzees and humans and gorillas. Differentially expressed genes were determined using a pseudo-bulk approach with DESeq2 and the Wald Test. Significantly enriched genes (adjusted p-value < 0.01) with greater than 0.5 log fold change expression in either species comparison were included. **(F)** Heatmap showing isoform proportions expressed in L2/3 IT neurons from two individuals per species for three genes (*BCAR1*, *INO80B*, and *SBNO1*) with human-specific switches in the main isoform. **(G)** Smart-seq v4 RNA-seq read pile-ups at the *INO80B* gene locus for L2/3 IT excitatory neurons in human, chimp, and gorilla. Read pile-ups are consistent with human neurons expressing both isoforms, while chimpanzee and gorilla neurons almost exclusively express the second isoform. This is consistent with the isoform proportions estimated using RSEM (see Methods) and visualized in Figure 2H. **(H)** A comparison of gene expression across cell subclasses between human and four NHP species. Boxplots (median, interquartile range - IQR, whiskers, +/- 1.5 IQR, and outliers) summarize the correlations for all one-to-one orthologous genes, and median correlation decreases with evolutionary distance from human. **(I)** Venn diagram of genes with subclass expression correlation < 0.25 between human and one or more species. **(J)** Expression dot plot of example genes with human- or ape-specific expression patterns.

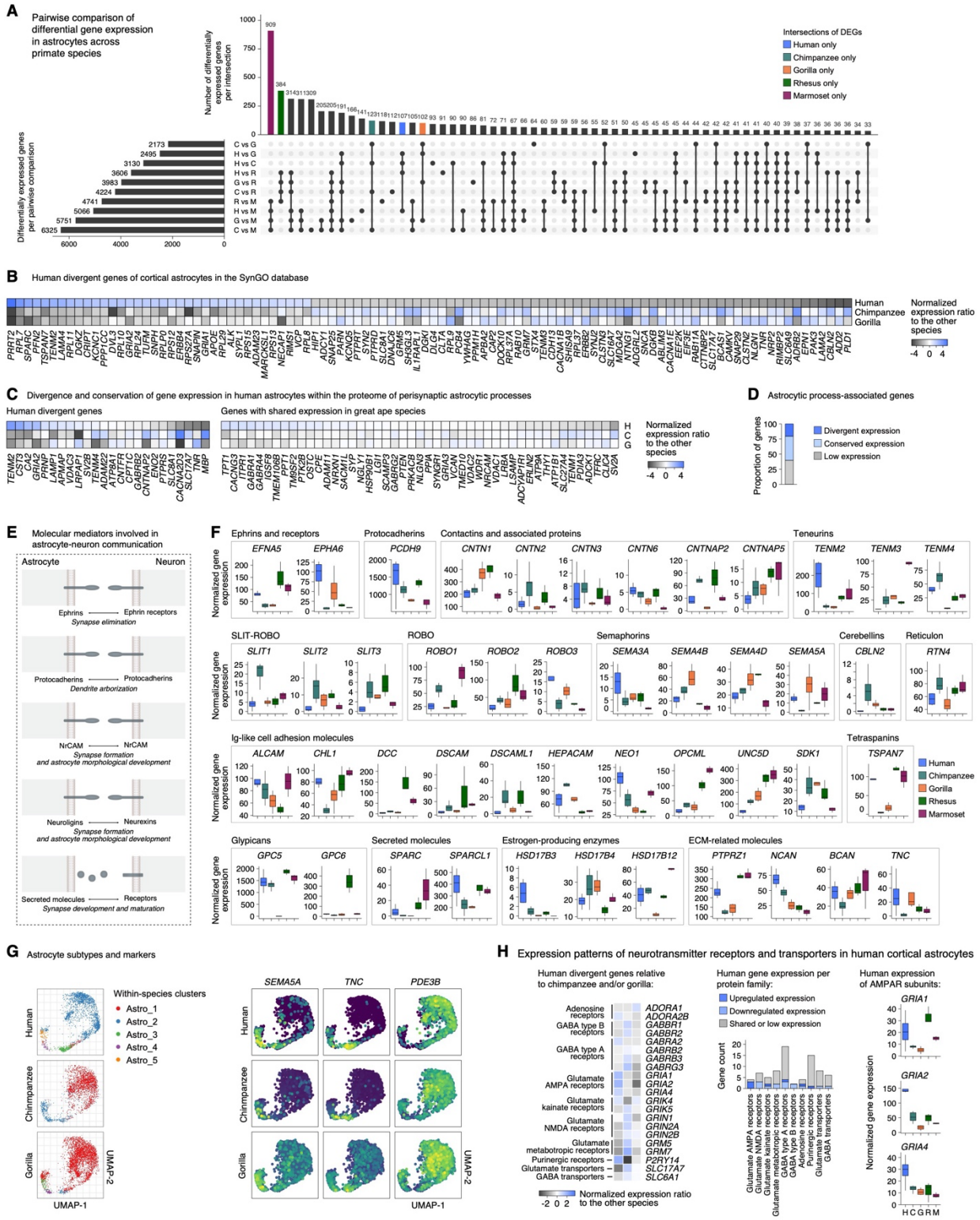

Fig. S5.

Divergent gene programs in astrocytes across great ape species. (A) Upset plot showing the number of DEGs in cortical astrocytes for pairwise comparisons between all primate species assayed in this study. **(B)** Heatmap showing astrocyte SynGO DEGs from the pairwise

comparison between human and chimpanzee and the pairwise comparison between human and gorilla (FDR < 0.01, top 100 DEGs visualized). Gene expression change is calculated as the log2 ratio of normalized expression counts in a given species relative to the other two species. **(C)** Heatmap showing genes of the proteome of perisynaptic astrocytic processes identified in (*29*) that have divergent expression (left) or conserved expression (right) in human astrocytes compared to chimpanzee and/or gorilla astrocytes (FDR < 0.01). **(D)** Proportion of genes enriched in astrocytic processes from (*29*) that show divergent, conserved or low expression in human astrocytes. **(E)** Schematics illustrating the trans-cellular interaction of molecular mediators involved in astrocyte-neuron communication (see (*77*) for details on specific molecular pathways mediating astrocytic development and function). **(F)** Examples of DEGs (FDR < 0.05) encoding cell-surface molecules involved in cell adhesion, astrocytic-secreted molecules, and extracellular matrix (ECM)-related molecules that show expression changes in cortical astrocytes across great ape species. **(G)** Markers and subtypes of cortical astrocytes across great ape species. **(H)** Divergent and shared expression of neurotransmitter receptors and transporters in cortical astrocytes. Left, heatmap showing the gene expression changes in human astrocytes compared to chimpanzee and gorilla astrocytes; middle, number of receptors or transporters per gene family that show divergent, shared, or low expression across great ape species; right, human-specific up-regulation of AMPA receptor subunit genes in astrocytes.

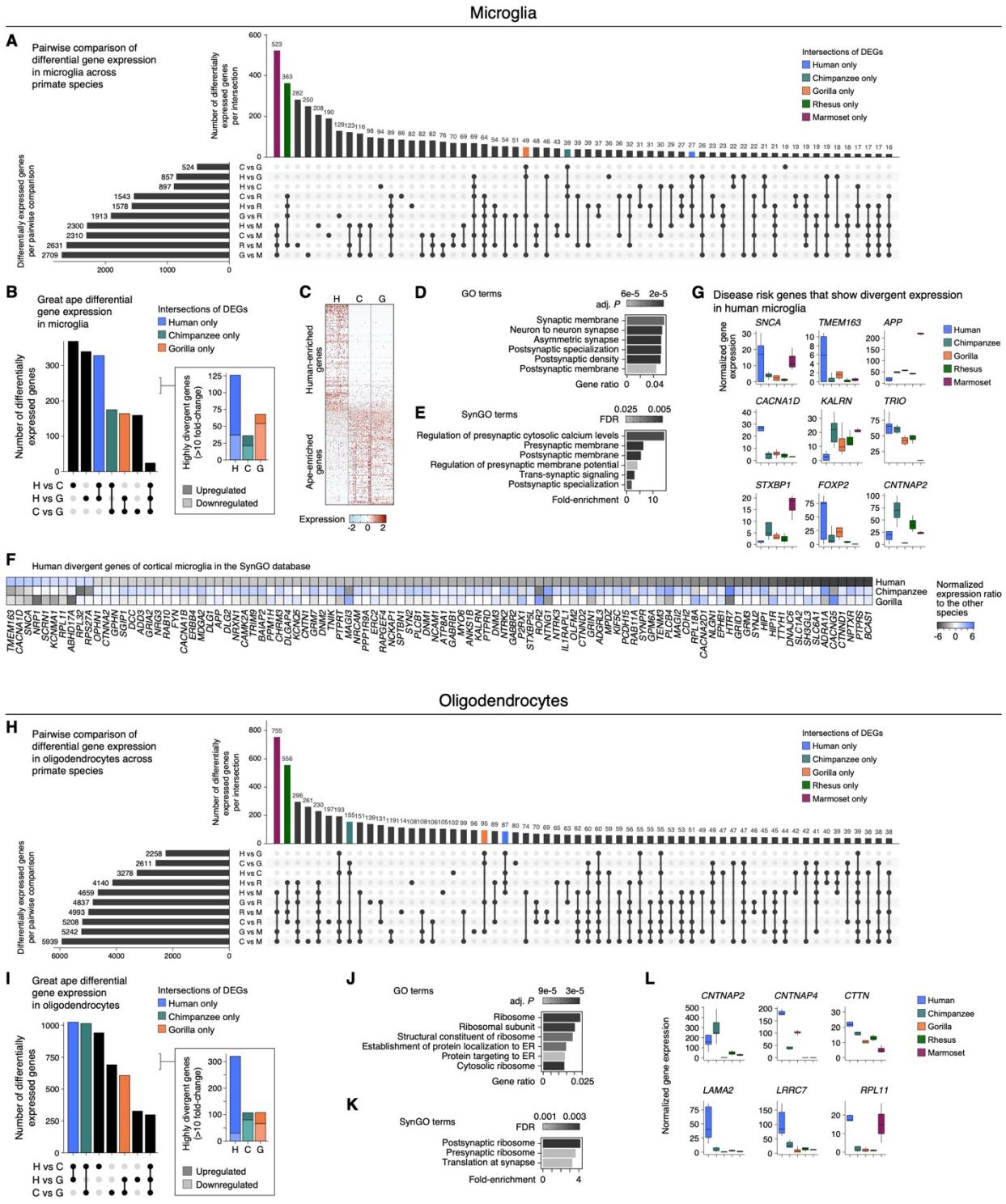

Fig. S6.

Divergent gene programs in microglia and oligodendrocytes across great ape species. (A) Upset plot showing the number of DEGs in cortical microglia for pairwise comparisons between all primate species assayed in this study. **(B)** Upset plot showing microglia DEGs for pairwise comparisons of great ape species. **(C)** Heatmap showing row-scaled expression of human versus chimpanzee and gorilla microglia DEGs. **(D-E)** Enrichment of select GO terms **(D)** and SynGO

terms **(E)** in the union of microglia DEGs from the pairwise comparison between human and chimpanzee and the pairwise comparison between human and gorilla (FDR < 0.05) that highlights genes related to synaptic processes, ribosomal machinery, and protein targeting pathways. **(F)** Heatmap showing microglia SynGO DEGs from the pairwise comparison between human and chimpanzee and the pairwise comparison between human and gorilla (FDR < 0.01; top 100 DEGs visualized). Gene expression change is calculated as the log2 ratio of normalized expression counts in a given species relative to the other two species. **(G)** Examples of disease-linked genes that show gene expression changes (FDR < 0.05) in human microglia compared to chimpanzee and gorilla microglia. **(H)** Upset plot showing the number of DEGs in cortical oligodendrocytes for pairwise comparisons between all primate species assayed in this study. **(I)** Upset plot showing oligodendrocyte DEGs across great ape species. **(J-K)** Enrichment of select GO **(K)** and SynGO **(L)** terms in the union of oligodendrocyte DEGs from the pairwise comparison between human and chimpanzee and the pairwise comparison between human and gorilla (FDR < 0.05). **(L)** Examples of DEGs (FDR < 0.01) related to myelin-axon interaction, cell adhesion, and translation that have undergone expression changes in great ape species.

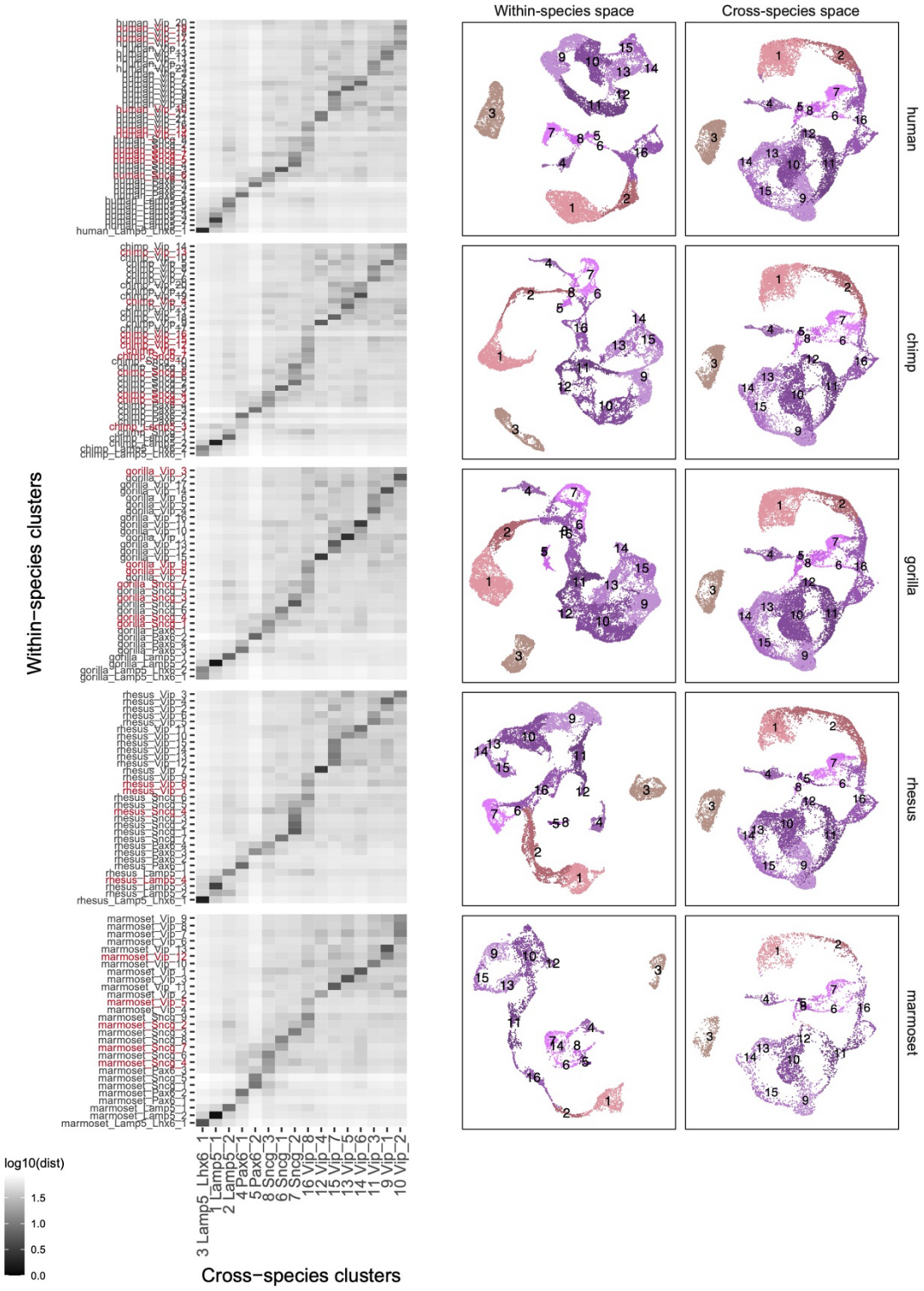

Fig. S7.
CGE-derived neuronal consensus types. Heatmaps of log-transformed Euclidean distances between within-species cluster centroids and cross-species consensus cluster centroids. Within-

species clusters with initial homologies across fewer than 5 species are labeled in red and were assigned to closely related cross-species clusters (see Methods). UMAPs of single nuclei from each species based on expression within species or integrated across all five species and labeled by cross-species cluster ids (listed as prefixes to cross-species cluster labels in heatmaps).

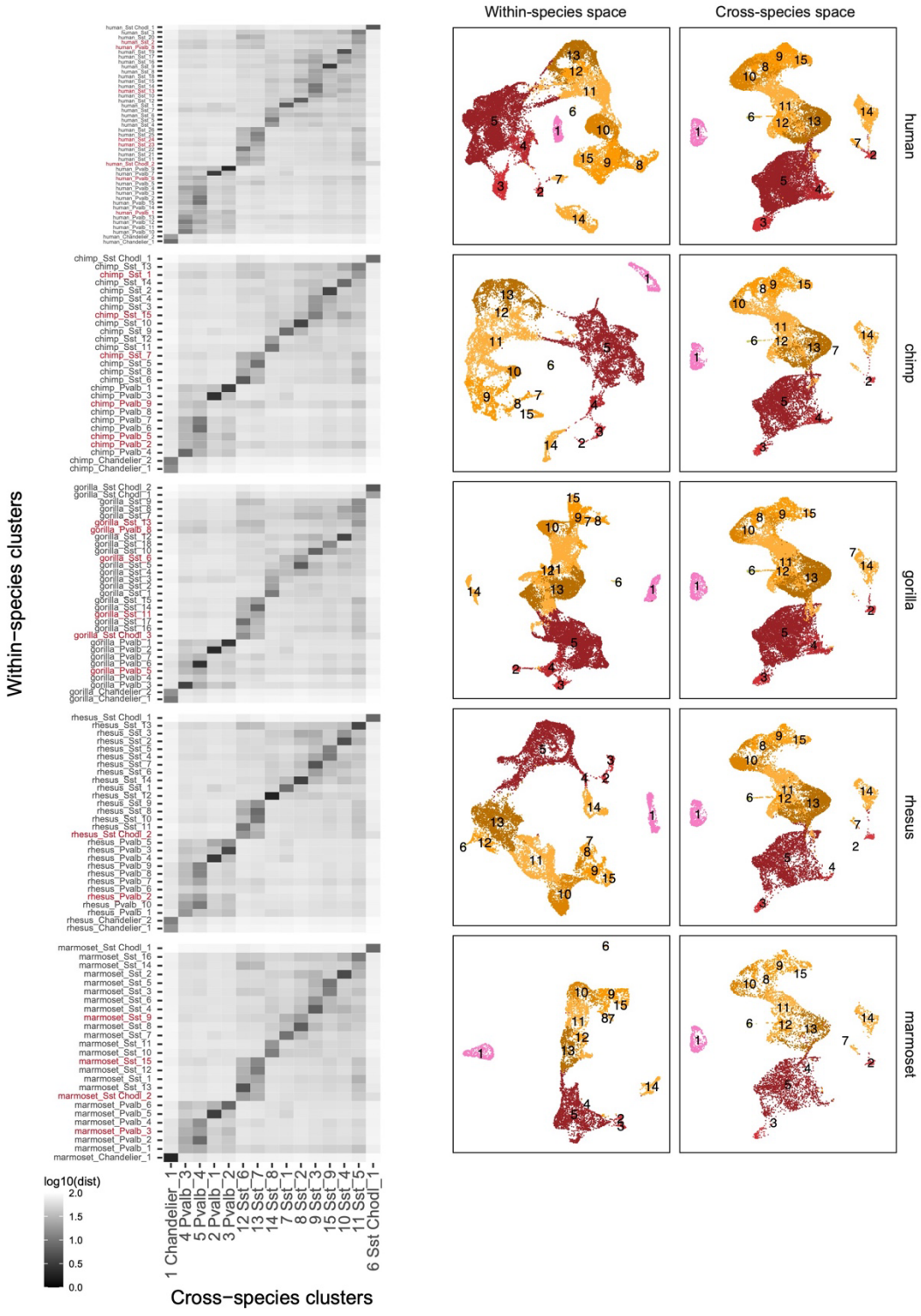

Fig. S8.
MGE-derived neuronal consensus types. Plots as described for CGE-derived types in **Fig. S7**.

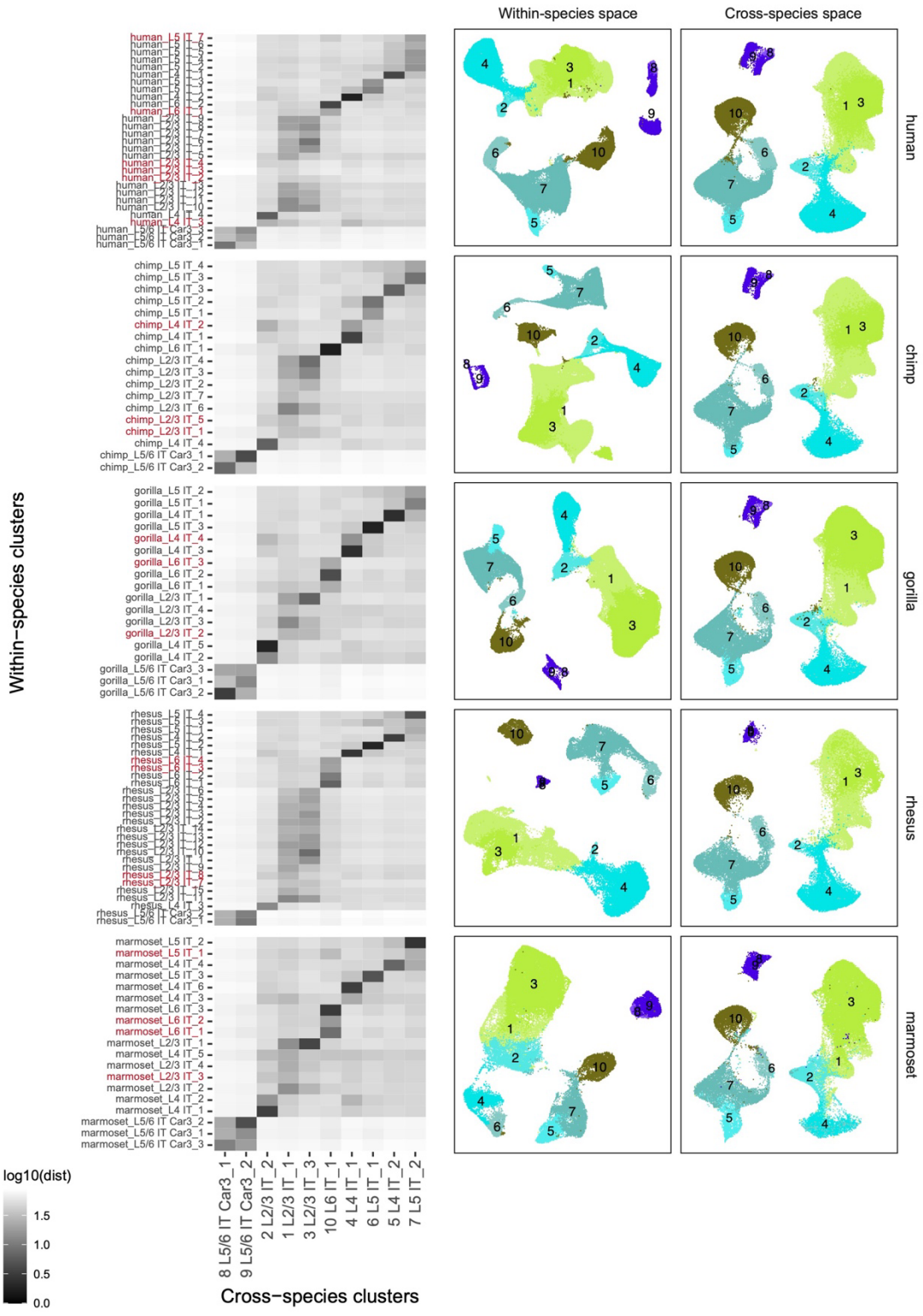

Fig. S9.
Intratelencephalic (IT)-projecting neuronal consensus types. Plots as described for CGE-derived types in **Fig. S7**.

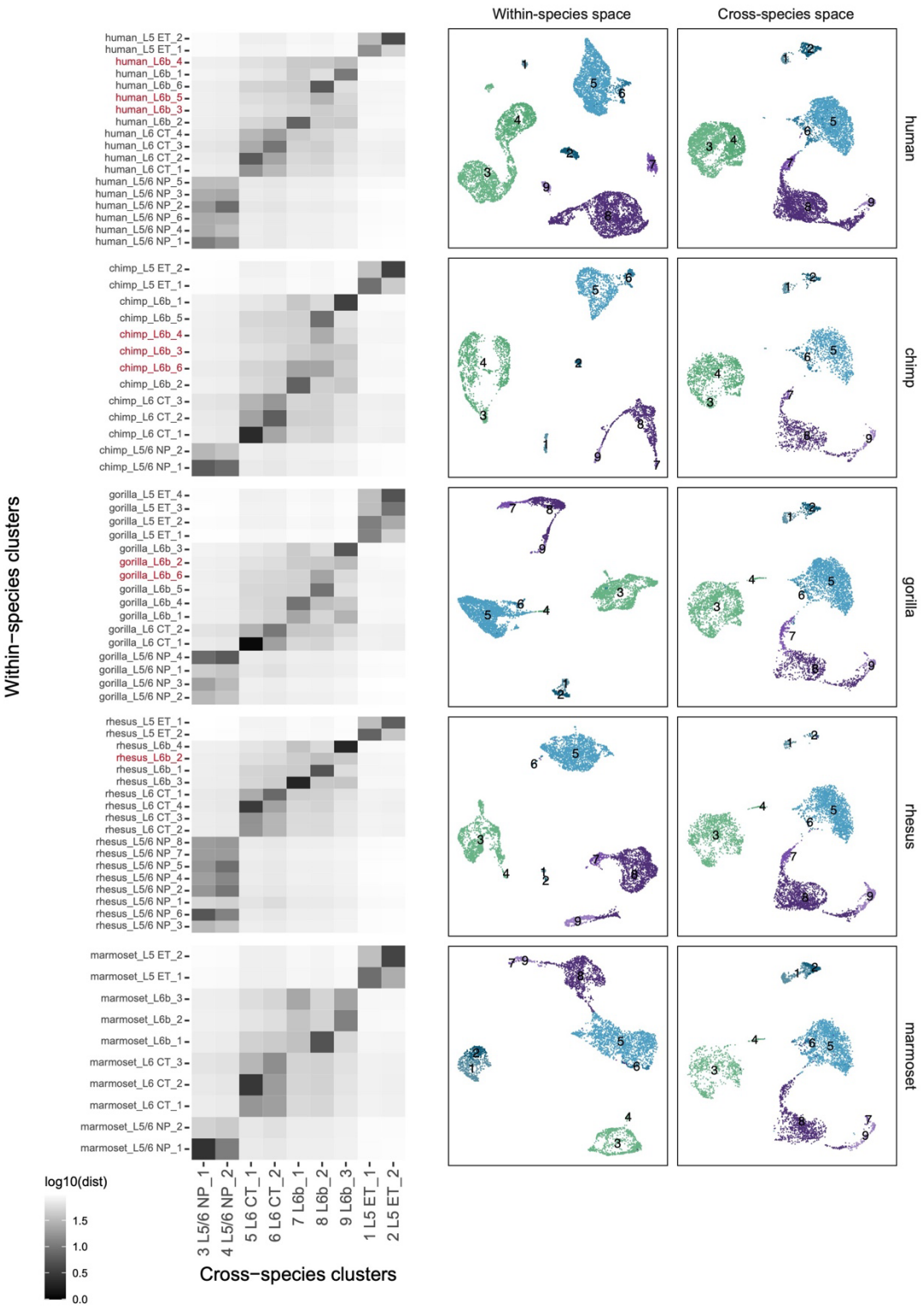

Fig. S10.
Non-IT-projecting neuronal consensus types. Plots as described for CGE-derived types in **Fig. S7**.

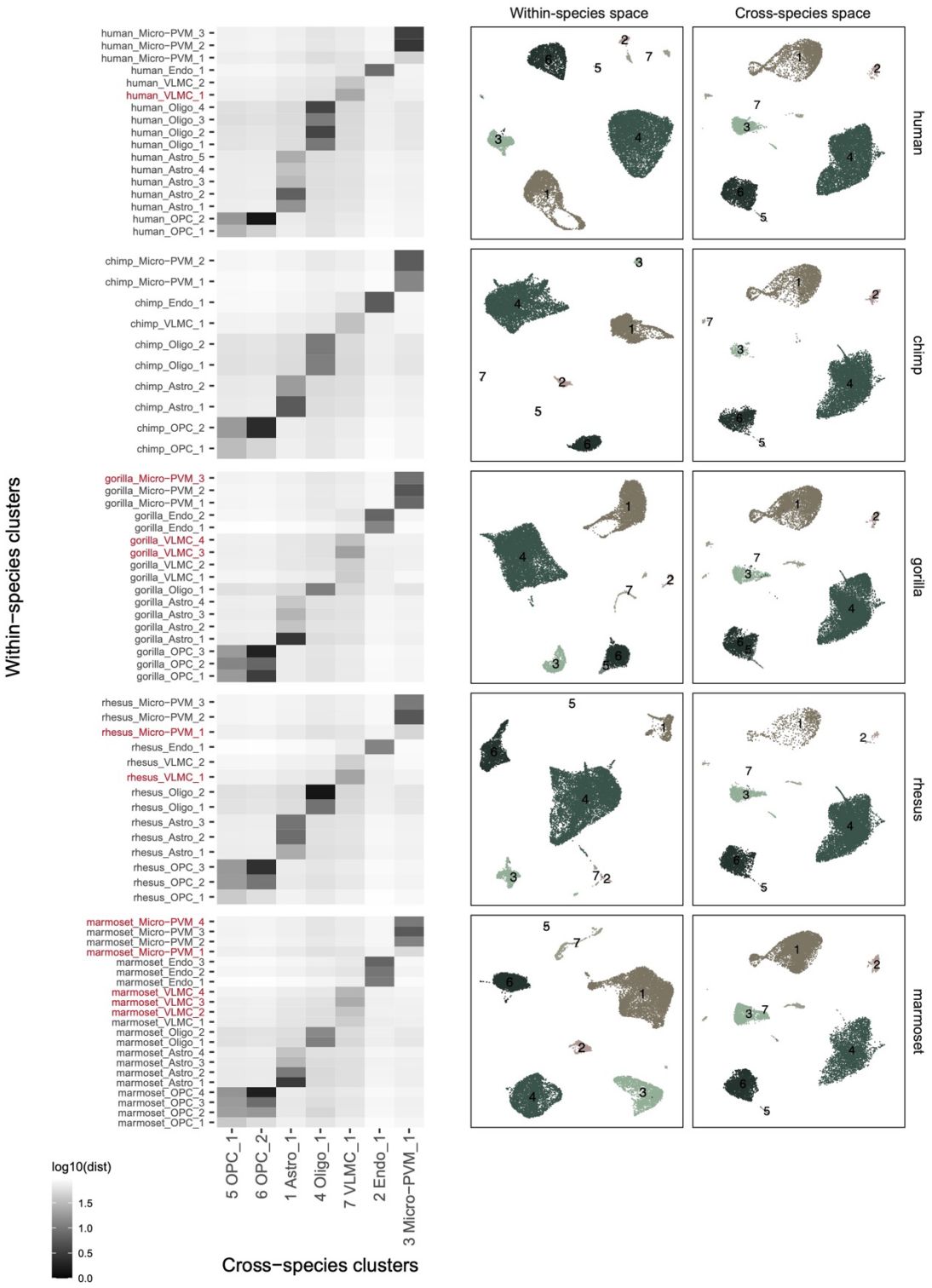

Fig. S11.
Non-neuronal consensus types. Plots as described for CGE-derived types in **Fig. S7**.

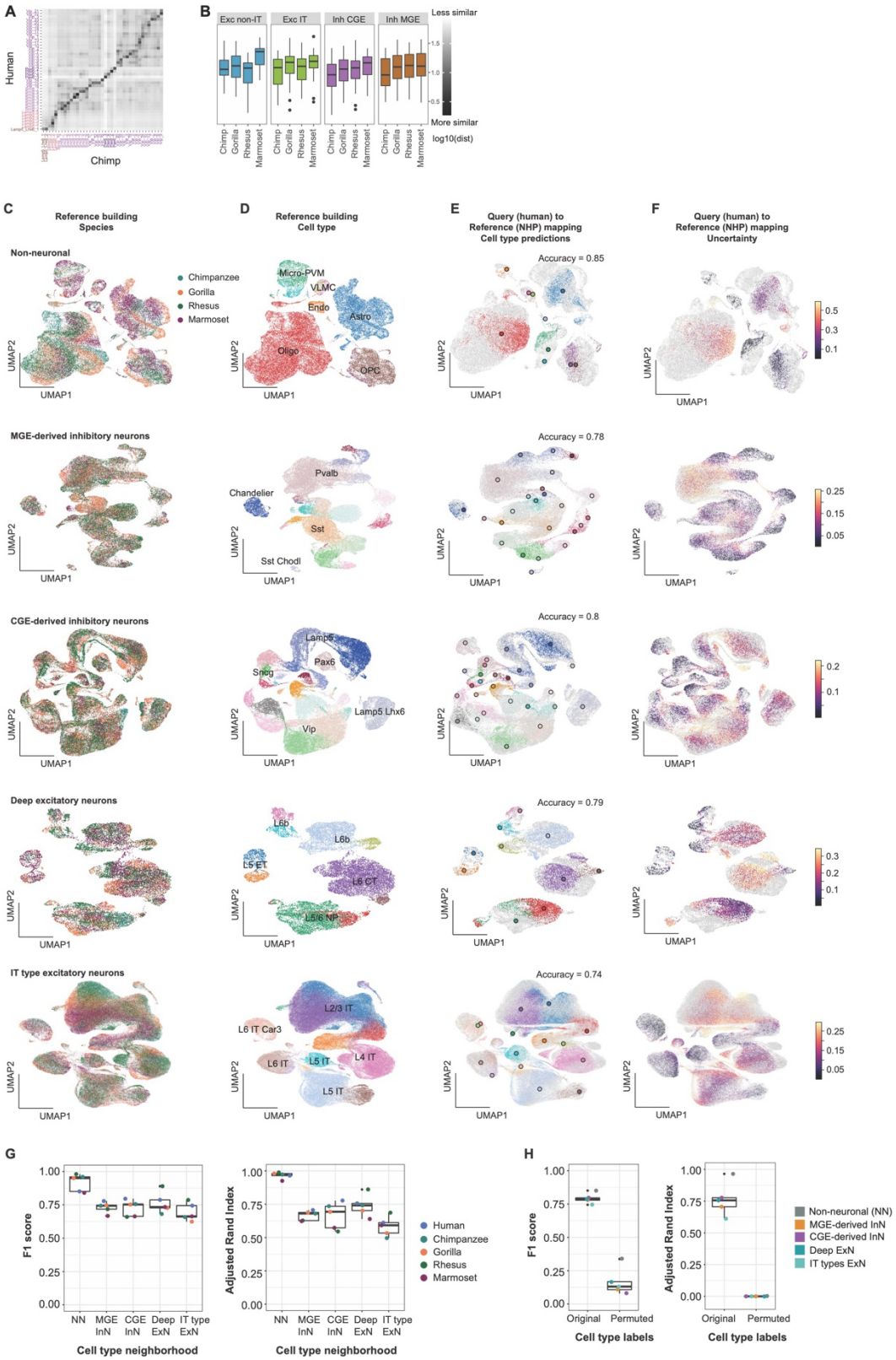

Fig. S12.

Cross-species consensus clustering. (A) Heatmap of the log-transformed Euclidean distance between human and chimpanzee cell type centroids shown in **Fig. 5B**. **(B)** Boxplots summarizing

the distance to each human cluster from the nearest corresponding NHP cluster for each pairwise species integration. **(C-F)** Using the scPoli framework, a reference dataset was built for each cell type neighborhood by integrating NHP MTG datasets, and learning prototypes of cell types in each integrated dataset. UMAPs of single nuclei from four NHP species to visualize integrated reference datasets are colored by **(C)** species, and **(D)** cell types for each of the five cell type neighborhoods. Nuclei in the query data (human MTG data split by neighborhood) are annotated by transferring the label of the closest cell type prototype in the corresponding reference dataset. UMAPs show the query datasets mapped to the reference data, with the query nuclei colored by **(E)** the predicted cell type (colors as in **(D)**) or reference nuclei from the four NHP species (gray points). Reference prototypes are indicated by circles with a black edge and colored by cell type. The accuracy of the label transfer is indicated at the top right corner of each UMAP. **(F)** UMAPs of the human and NHP reference integrated datasets with human query nuclei colored by classification uncertainty and reference nuclei colored in gray. **(G)** Boxplots show the cell type classification performance on different query datasets split by neighborhood. Cell type labels predicted by scPoli are largely consistent with those derived from MetaNeighbor as observed by the high (left) F1 score, and (right) adjusted rand index across cell type neighborhoods and query datasets. **(H)** Cell type classification performance measured by (left) F1 score, and (right) adjusted rand index, when labeling query nuclei (human MTG) with or without permuted cell type labels. Reduced scores with permuted labels confirms that similar clusters were detected by MetaNeighbor and scPoli.

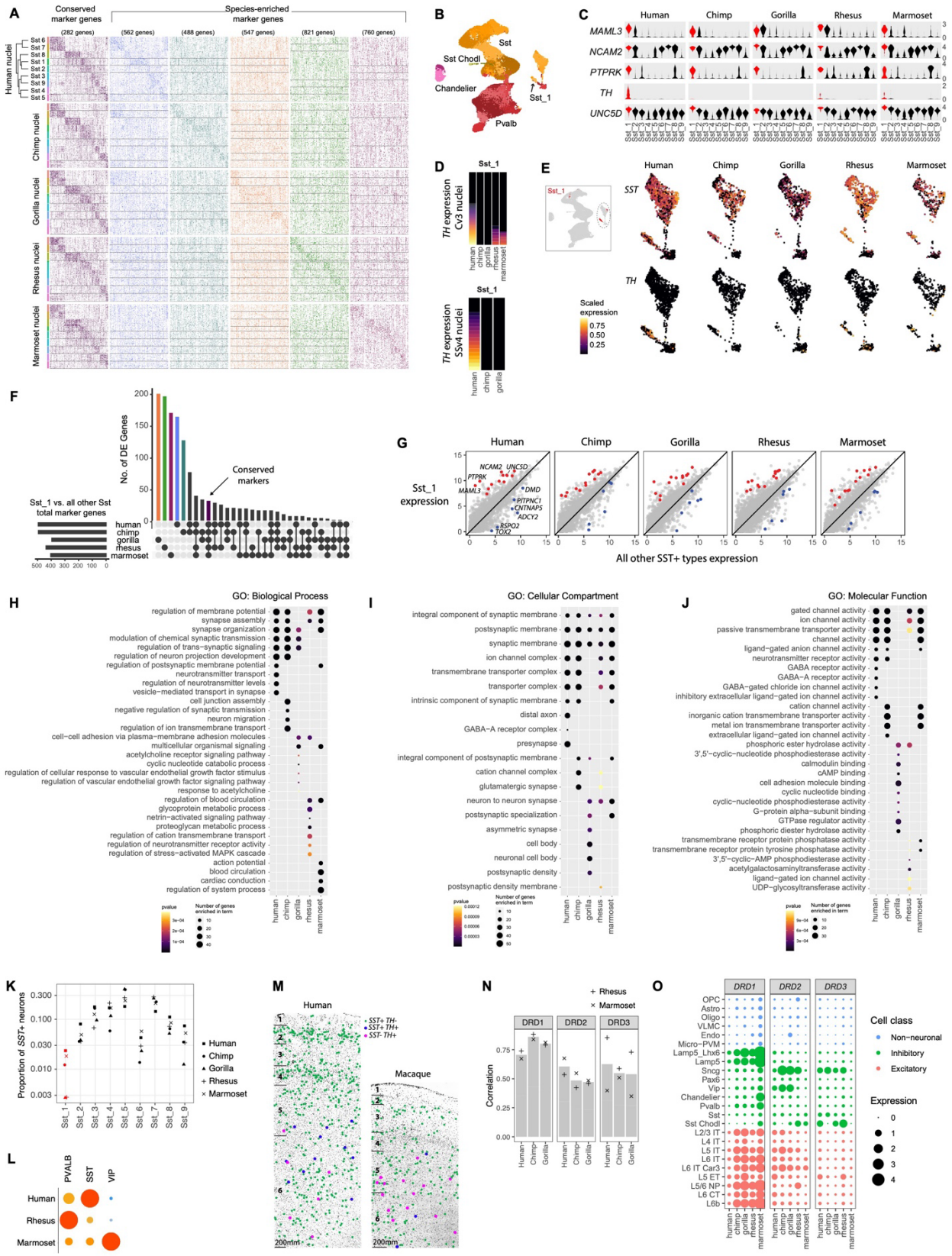
A
Conserved marker genes
Species-enriched marker genes
(282 genes)
(562 genes)
(488 genes)
(547 genes)
(821 genes)
(760 genes)
Human nuclei
Chimp nuclei
Gorilla nuclei
Rhesus nuclei
Marmoset nuclei
B
Sst
Sst Chodl
Chandelier
Pvalb
Sst_1
C
Human
Chimp
Gorilla
Rhesus
Marmoset
MAML3
NCAM2
PTPRK
TH
UNC5D
D
Sst_1
TH expression CV3 nuclei
TH expression SSv4 nuclei
human
chimp
gorilla
rhesus
marmoset
E
Sst_1
SST
TH
Scaled expression
0.75
0.50
0.25
F
No. of DE Genes
Conserved markers
Sst_1 vs. all other Sst total marker genes
human
chimp
gorilla
rhesus
marmoset
G
Human
Chimp
Gorilla
Rhesus
Marmoset
Sst_1 expression
NCAM2
UNC5D
PTPRK
MAML3
DMD
PITPNC1
CNTNAP5
ADCY2
RSPO2
TOX2
All other SST+ types expression
H
GO: Biological Process
regulation of membrane potential
synapse assembly
synapse organization
modulation of chemical synaptic transmission
regulation of trans-synaptic signaling
regulation of neuron projection development
regulation of postsynaptic membrane potential
neurotransmitter transport
regulation of neurotransmitter levels
vesicle-mediated transport in synapse
cell junction assembly
negative regulation of synaptic transmission
neuron migration
regulation of ion transmembrane transport
cell-cell adhesion via plasma-membrane adhesion molecules
multicellular organismal signaling
acetylcholine receptor signaling pathway
cyclic nucleotide catabolic process
regulation of cellular response to vascular endothelial growth factor stimulus
regulation of vascular endothelial growth factor signaling pathway
response to acetylcholine
regulation of blood circulation
glycoprotein metabolic process
netrin-activated signaling pathway
proteoglycan metabolic process
regulation of cation transmembrane transport
regulation of neurotransmitter receptor activity
regulation of stress-activated MAPK cascade
action potential
blood circulation
cardiac conduction
regulation of system process
pvalue
Number of genes enriched in term
I
GO: Cellular Compartment
integral component of synaptic membrane
postsynaptic membrane
synaptic membrane
ion channel complex
transmembrane transporter complex
transporter complex
intrinsic component of synaptic membrane
distal axon
GABA-A receptor complex
presynapse
integral component of postsynaptic membrane
cation channel complex
glutamatergic synapse
neuron to neuron synapse
postsynaptic specialization
asymmetric synapse
cell body
neuronal cell body
postsynaptic density
postsynaptic density membrane
J
GO: Molecular Function
gated channel activity
ion channel activity
passive transmembrane transporter activity
channel activity
ligand-gated anion channel activity
neurotransmitter receptor activity
GABA receptor activity
GABA-A receptor activity
GABA-gated chloride ion channel activity
inhibitory extracellular ligand-gated ion channel activity
cation channel activity
inorganic cation transmembrane transporter activity
metal ion transmembrane transporter activity
extracellular ligand-gated ion channel activity
phosphoric ester hydrolase activity
3',5'-cyclic-nucleotide phosphodiesterase activity
calmodulin binding
cAMP binding
cell adhesion molecule binding
cyclic nucleotide binding
cyclic-nucleotide phosphodiesterase activity
G-protein alpha-subunit binding
GTPase regulator activity
phosphoric diester hydrolase activity
transmembrane receptor protein phosphatase activity
transmembrane receptor protein tyrosine phosphatase activity
3',5'-cyclic-AMP phosphodiesterase activity
acetylgalactosaminyltransferase activity
ligand-gated ion channel activity
UDP-glycosyltransferase activity
K
Proportion of SST+ neurons
Human
Chimp
Gorilla
Rhesus
Marmoset
L
PVALB
SST
VIP
Human
Rhesus
Marmoset
M
Human
SST+ TH-
SST+ TH+
SST- TH+
Macaque
200mm
N
Rhesus
Marmoset
DRD1
DRD2
DRD3
Correlation
O
DRD1
DRD2
DRD3
OPC
Astro
Oligo
VLMC
Endo
Micro-PVM
Lamp5_Lhx6
Lamp5
Sncg
Pax6
Vip
Chandelier
Pvalb
Sst
Sst Chodl
L2/3 IT
L4 IT
L5 IT
L6 IT
L6 IT Car3
L5 ET
L5/6 NP
L6 CT
L6b
Cell class
Non-neuronal
Inhibitory
Excitatory
Expression

Fig. S13.
Conserved SST-expressing interneuron type lacks TH expression in chimpanzees and gorillas. (A) Conserved and species-enriched markers of SST-expressing consensus interneuron types (**Table S5**). **(B)** UMAP of human MGE-derived interneurons colored by cluster and labeled with major subclasses. Sst_1 labels the SST+/TH+ type. **(C)** Distribution of expression values for marker genes of the Sst_1 cluster (red) versus all other SST-expressing types. **(D)** Stacked bar plots of TH expression measured by droplet-based 3'-UTR sequencing (Cv3) and full length transcript sequencing (SSv4) show no expression detected in chimpanzee and gorilla Sst_1 neurons. **(E)** Inset: UMAP of MGE-derived interneurons integrated across species and colored by Sst_1 cluster membership. Expanded view of SST and TH expression in each species shown for Sst_1 and related types. **(F)** Upset plot summarizing intersections of Sst_1 marker genes across species. A minority of markers are conserved across the five species. **(G)** Average of expression of Sst_1 neurons versus all other SST-expressing types in each species with conserved up-regulated (red) and down-regulated (blue) markers highlighted. **(H-J)** Top enriched GO terms for biological process (H), cellular component (I), and molecular function (J) for species-enriched markers of the Sst_1 type. A minority of terms are significant in all species, and most are species-specific. **(K)** Proportions of SST consensus types among SST-expressing interneurons for each species. Sst_1 neurons are highlighted and range from 0.3–3% of SST+ interneurons. **(L)** Relative proportions (normalized within species) of *PVALB*, *SST*, and *VIP* interneurons that express *TH* in human, macaque, and marmoset. Maximum relative expression is indicated by dot color from low (blue) to high (red). **(M)** *In situ* labeling of cells based on co-expression of *SST* and *TH* in human and macaque MTG using RNAScope. **(N)** Spearman correlations of dopamine receptor subtype (DRD1, DRD2, and DRD3) expression levels across cell subclasses between each great ape species and rhesus and marmoset. Bar plots denote mean correlations for each species and gene, and correlations were not significantly different across species. **(O)** Expression of three dopamine receptor subtypes across cell subclasses and species.

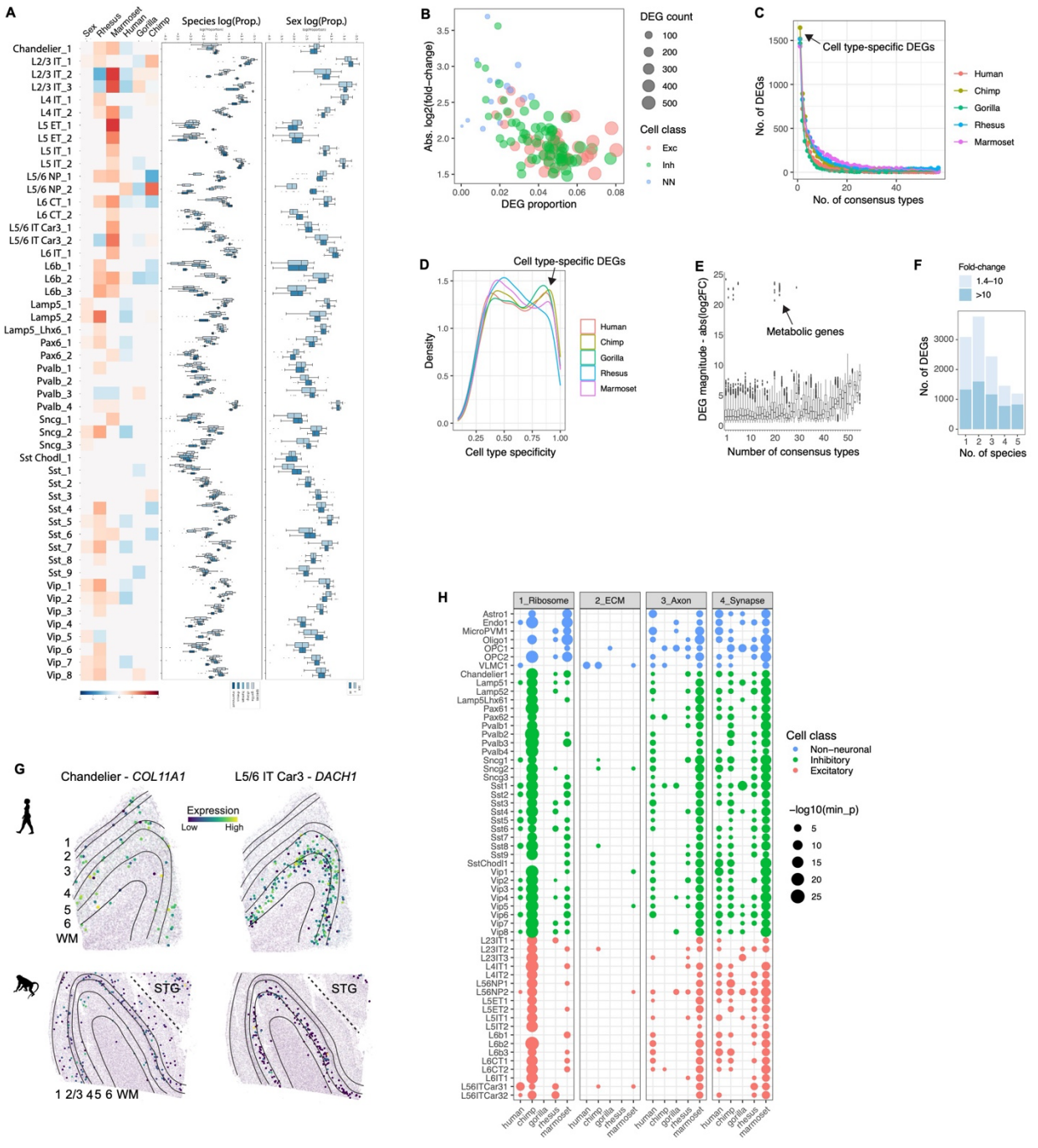

Fig. S14.

Divergent expression of consensus cell types. (A) scCODA compositional analysis showing neuronal consensus types that change proportions across sex or species. **(B)** For consensus type DEGs in humans versus all other species (hDEGs), median log-transformed absolute fold-changes are plotted versus the DEG proportion of median expressed genes in each type. The absolute number of DEGs and cell class are indicated by point size and color, respectively. **(C)** Distributions of the number of species DEGs that are differentially expressed across different numbers of consensus types. Most DEGs are specific to one or a few consensus types. **(D)** Cell type specificities (tau) of genes in each species that are differentially expressed in at least one

type. A tau score of 0 indicates expression is evenly distributed across types, and 1 indicates a binary marker expressed in a single type. More recent evolutionary changes among great apes tend to be more cell type-specific. **(E)** Distribution of absolute fold-change in expression for human DEGs that are grouped by the number of consensus types that show differential expression for those DEGs. Genes that are DEGs in most or all cell types have larger changes in expression. **(F)** Highly divergent (>10-fold change) DEGs are often differentially expressed in multiple species. **(G)** MERFISH validation of human-enriched expression in Chandelier interneurons and L5/6 IT Car3 excitatory neurons. **(H)** Dot plots of consensus types that have significant GO enrichment of DEGs for each species. Dot size denotes the negative log-transformed minimum nominal p-value across all GO terms associated with the four GO categories (ribosome, ECM, axon, and synapse) from **Figure 5**.

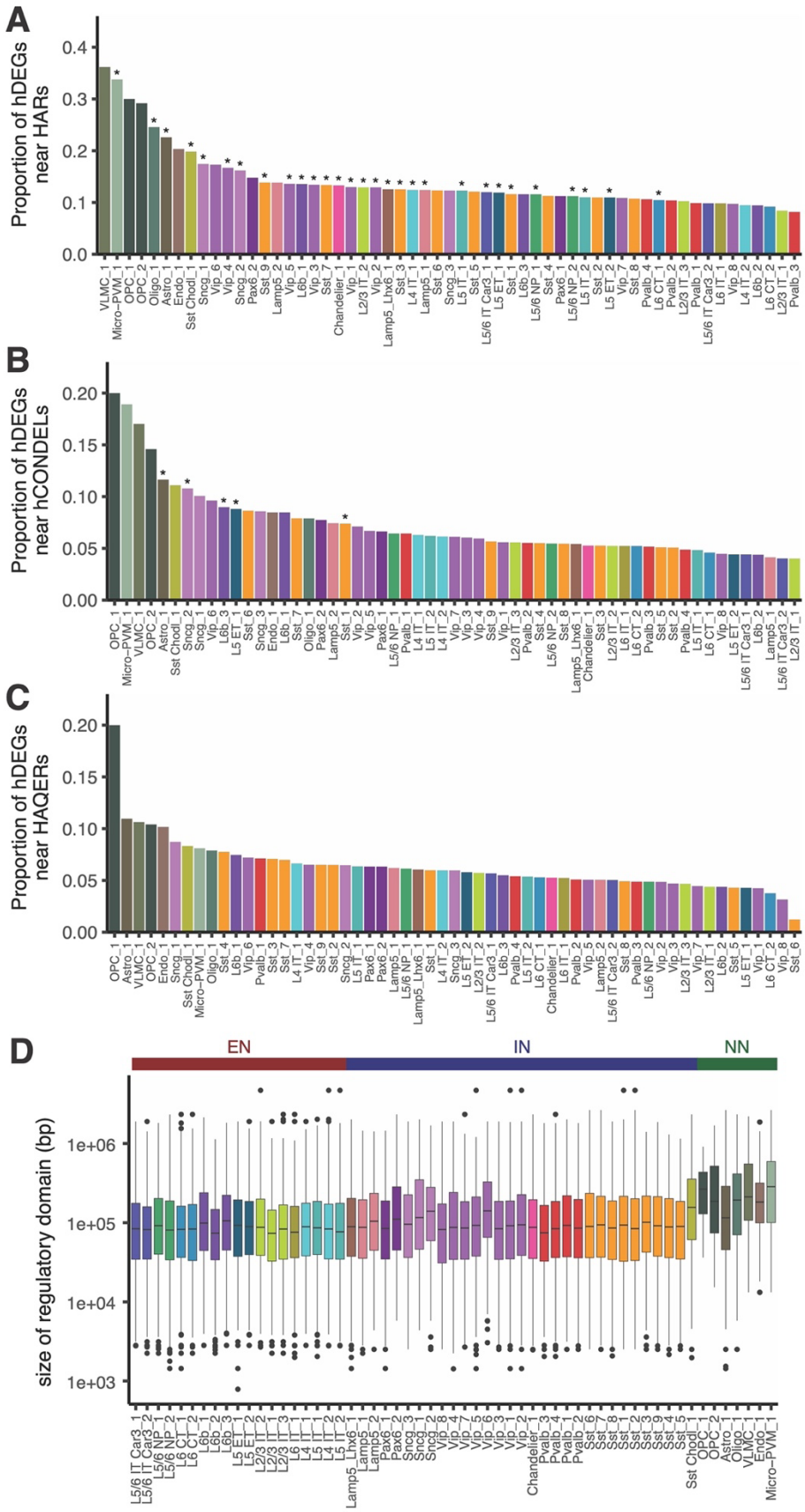
A
Proportion of hDEGs near HARs
0.0
0.1
0.2
0.3
0.4
VLMC_1
Micro−PVM_1
OPC_1
OPC_2
Oligo_1
Astro_1
Endo_1
Sst Chodl_1
Sncg_1
Vip_6
Vip_4
Sncg_2
Pax6_2
Sst_9
Lamp5_2
Vip_5
L6b_1
Vip_3
Sst_7
Chandelier_1
Vip_1
L2/3 IT_2
Vip_2
Lamp5_Lhx6_1
Sst_3
L4 IT_1
Lamp5_1
Sst_6
Sncg_3
L5 IT_1
Sst_5
L5/6 IT Car3_1
L5 ET_1
Sst_1
L6b_3
L5/6 NP_1
Sst_4
Pax6_1
L5/6 NP_2
L5 IT_2
Sst_2
L5 ET_2
Vip_7
Sst_8
Pvalb_4
L6 CT_1
Pvalb_2
L2/3 IT_3
Pvalb_1
L5/6 IT Car3_2
L6 IT_1
Vip_8
L4 IT_2
L6b_2
L6 CT_2
L2/3 IT_1
Pvalb_3
B
Proportion of hDEGs near hCONDELs
0.00
0.05
0.10
0.15
0.20
OPC_1
Micro−PVM_1
VLMC_1
OPC_2
Astro_1
Sst Chodl_1
Sncg_1
Sncg_2
Vip_6
L6b_3
L5 ET_1
Sst_6
Sncg_3
Endo_1
L6b_1
Sst_7
Oligo_1
Pax6_2
Lamp5_2
Sst_1
Vip_2
Vip_5
Pax6_1
L5/6 NP_1
Pvalb_1
L4 IT_1
L5 IT_2
L4 IT_2
Vip_7
Vip_3
Vip_4
Sst_9
Vip_1
L2/3 IT_3
Pvalb_2
Sst_4
L5/6 NP_2
Sst_8
Lamp5_Lhx6_1
Chandelier_1
Sst_3
L2/3 IT_2
L6 IT_1
L6 CT_2
Pvalb_3
Sst_5
Sst_2
Pvalb_4
L5 IT_1
L6 CT_1
Vip_8
L5 ET_2
L5/6 IT Car3_1
L6b_2
Lamp5_1
L5/6 IT Car3_2
L2/3 IT_1
C
Proportion of hDEGs near HAQERs
0.00
0.05
0.10
0.15
0.20
OPC_1
Astro_1
VLMC_1
OPC_2
Endo_1
Sncg_1
Sst Chodl_1
Micro−PVM_1
Oligo_1
Sst_4
L6b_1
Vip_6
Pvalb_1
Sst_3
Sst_7
L4 IT_1
Vip_4
Sst_9
Sst_2
Sncg_2
L5 IT_1
Pax6_1
Pax6_2
Lamp5_1
L5/6 NP_1
Lamp5_Lhx6_1
Sst_1
L4 IT_2
Sncg_3
L5 ET_2
L2/3 IT_2
L5/6 IT Car3_1
L6b_3
Pvalb_4
L5 IT_2
L6 CT_1
Chandelier_1
L6 IT_1
Pvalb_2
Vip_5
Lamp5_2
L5/6 IT Car3_2
Sst_8
Pvalb_3
L5/6 NP_2
Vip_2
Vip_3
L2/3 IT_3
Vip_7
L2/3 IT_1
L6b_2
Sst_5
L5 ET_1
Vip_1
L6 CT_2
Vip_8
Sst_6
D
EN
IN
NN
size of regulatory domain (bp)
1e+03
1e+04
1e+05
1e+06
L5/6 IT Car3_1
L5/6 IT Car3_2
L5/6 NP_2
L5/6 NP_1
L6 CT_1
L6 CT_2
L6b_1
L6b_2
L6b_3
L5 ET_1
L5 ET_2
L2/3 IT_2
L2/3 IT_3
L4 IT_1
L4 IT_2
L5 IT_1
L5 IT_2
Lamp5_Lhx6_1
Lamp5_1
Lamp5_2
Pax6_1
Pax6_2
Sncg_1
Sncg_2
Sncg_3
Vip_8
Vip_7
Vip_4
Vip_5
Vip_6
Vip_3
Vip_1
Vip_2
Chandelier_1
Pvalb_3
Pvalb_4
Pvalb_1
Pvalb_2
Sst_6
Sst_7
Sst_8
Sst_1
Sst_2
Sst_3
Sst_9
Sst_4
Sst_5
Sst Chodl_1
OPC_1
OPC_2
Astro_1
Oligo_1
VLMC_1
Endo_1
Micro−PVM_1

Fig. S15.
hDEGs are enriched near HARs and hCONDELs, but not HAQERs. HARs **(A)** and hCONDELs **(B)** are enriched near hDEGs in some consensus cell types. HAQERs **(C)** are not enriched near hDEGs in any consensus cell types. Asterisks indicate significance at 5% FDR for both (1) Fisher's exact test to test for over-representation of hDEGs near HARs, hCONDELs, or HAQERs compared to all expressed genes, and (2) the binomial test to account for differences in the size of regulatory domains (*87*). **(C)** Box plots (median and interquartile range (IQR), outliers exceed 1.5 * IQR) of the size distribution of regulatory domains for hDEGs in each consensus type. The regulatory domain for each gene is defined as its intronic regions and its flanking intergenic regions. Non-neuronal hDEGs have large gene regulatory domains. EN: excitatory neuron. IN: inhibitory neuron. NN: non-neuronal.

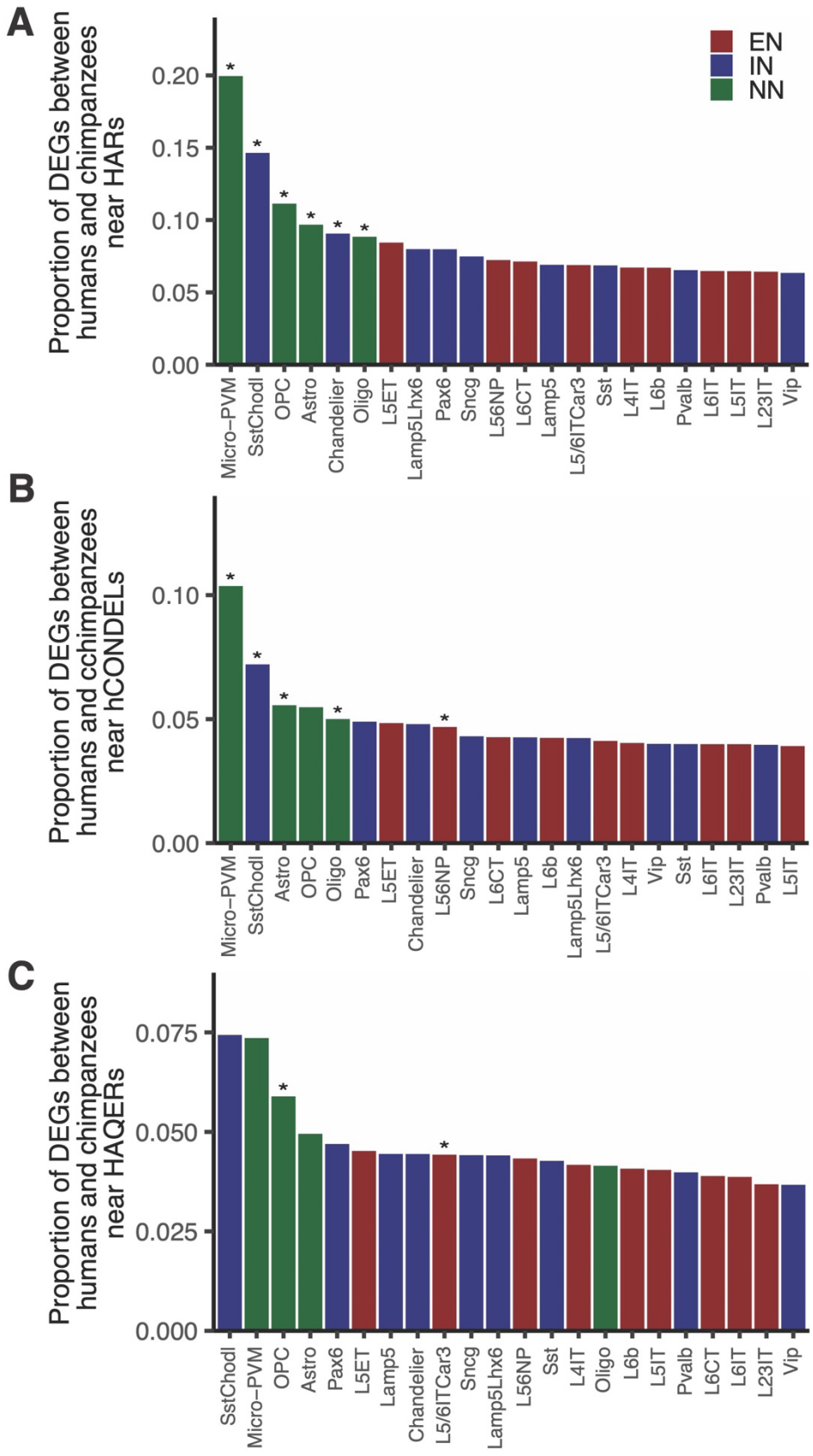
A
Proportion of DEGs between humans and chimpanzees near HARs
0.20
0.15
0.10
0.05
0.00
EN
IN
NN
Micro–PVM
SstChodl
OPC
Astro
Chandelier
Oligo
L5ET
Lamp5Lhx6
Pax6
Sncg
L56NP
L6CT
Lamp5
L5/6ITCar3
Sst
L4IT
L6b
Pvalb
L6IT
L5IT
L23IT
Vip
B
Proportion of DEGs between humans and cchimpanzees near hCONDELs
0.10
0.05
0.00
Micro–PVM
SstChodl
Astro
OPC
Oligo
Pax6
L5ET
Chandelier
L56NP
Sncg
L6CT
Lamp5
L6b
Lamp5Lhx6
L5/6ITCar3
L4IT
Vip
Sst
L6IT
L23IT
Pvalb
L5IT
C
Proportion of DEGs between humans and chimpanzees near HAQERs
0.075
0.050
0.025
0.000
SstChodl
Micro–PVM
OPC
Astro
Pax6
L5ET
Lamp5
Chandelier
L5/6ITCar3
Sncg
Lamp5Lhx6
L56NP
Sst
L4IT
Oligo
L6b
L5IT
Pvalb
L6CT
L6IT
L23IT
Vip

Fig. S16.
Enrichment of human (H), chimpanzee (C), gorilla (G), and rhesus macaque (R) DEGs near HARs and/or hCONDELs across consensus cell types. (A) Size of each dot is the proportion of species-specific DEGs near HARs and/or hCONDELs, and the color indicates the adjusted p-values. Associations were considered significant if both (1) Fisher's exact test to test for over-representation of DEGs between humans and chimpanzees near HARs, hCONDELs, or HAQERs compared to all expressed genes and (2) the binomial test to account for differences in the size of regulatory domains on the likelihood that HARs, hCONDELs, or HAQERs would be near a given gene were both significant at 5% FDR (*87*). Gray dots are not significant. The less significant of the two adjusted p-values between the Fisher's exact test and the binomial test is plotted. Bar plots on the right display the number of consensus cell types for each species where DEGs are significantly enriched near HARs and/or hCONDELs. **(B)** Scatterplots comparing the proportion of chimpanzee, gorilla, or rhesus macaque DEGs near HARs or hCONDELs to the proportion of human DEGs near HARs or hCONDELs. Dots are colored by whether they are significant in humans and/or the other non-human primate species.

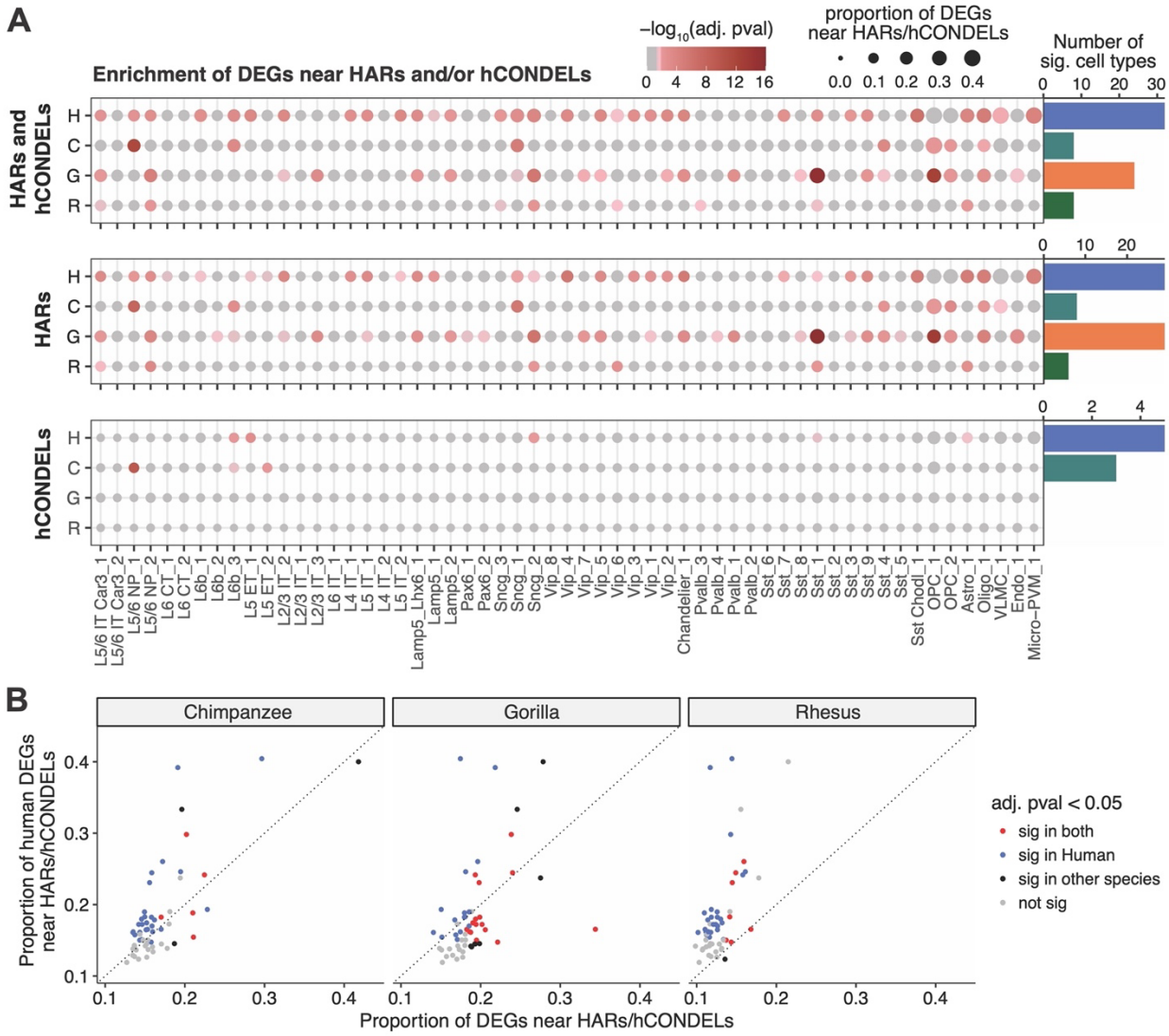

Fig. S17.
Enrichment of DEGs between humans and chimpanzees near HARs (A), hCONDELs (B), and HAQERs (C) for cell subclasses. Asterisks indicate significance at 5% FDR for both (1) Fisher's exact test to test for over-representation of DEGs between humans and chimpanzees near HARs, hCONDELs, or HAQERs compared to all expressed genes and (2) the binomial test to account for differences in the size of regulatory domains on the likelihood that HARs, hCONDELs, or HAQERs would be near a given gene (*87*). EN: excitatory neuron. IN: inhibitory neuron. NN: non-neuronal.

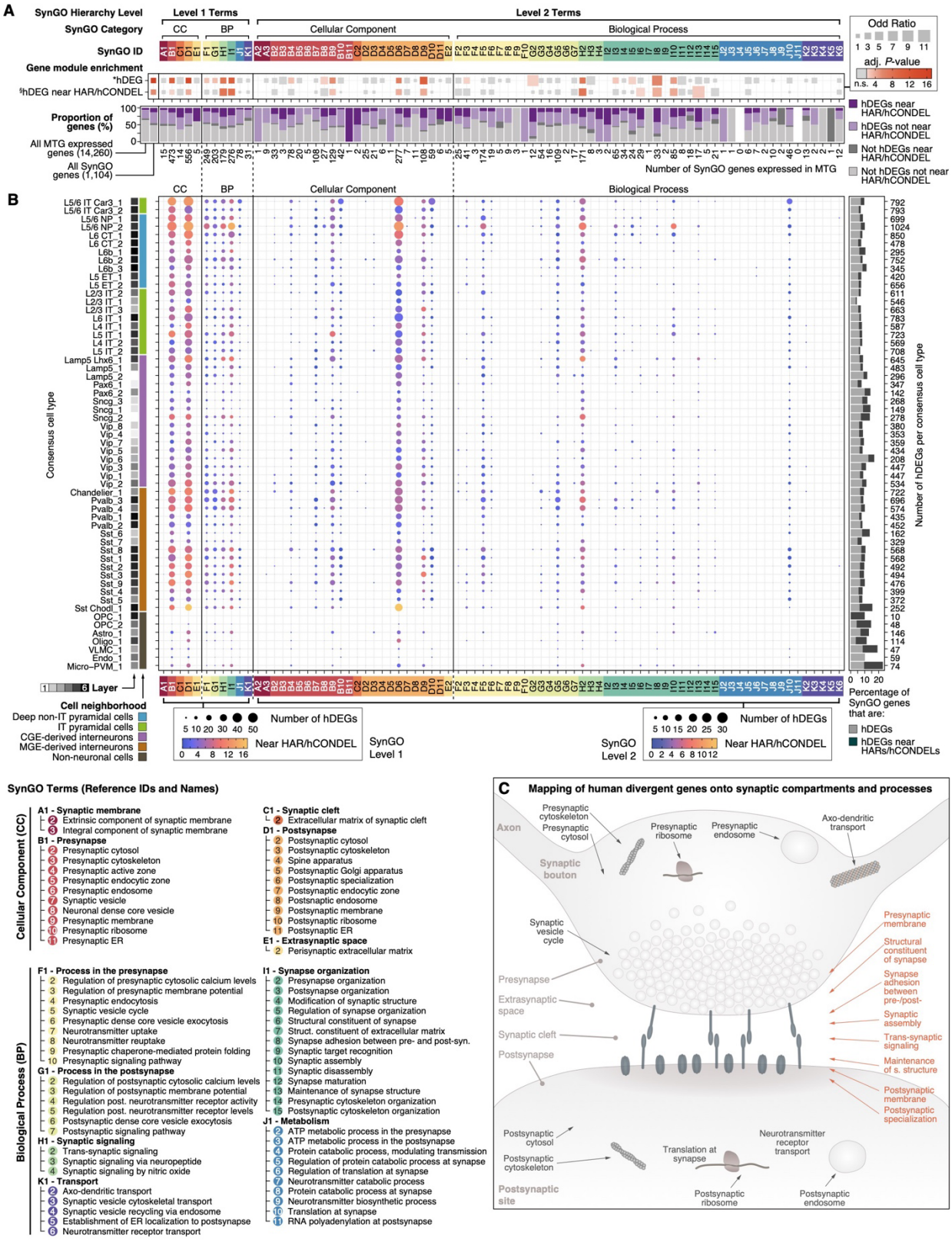

Fig. S18.

Expanded summary of hDEG enrichment near HARs or hCONDELs in SynGO. The proportion of genes that are hDEGs and/or near HARs or hCONDELs is plotted for all genes

expressed in the MTG, all genes annotated in SynGO (*28*), and genes annotated to specific SynGO terms (**Table S8**) either aggregated across consensus cell types **(A)** or for each individual consensus cell type **(B)**. *Fisher's exact test of whether hDEGs are enriched for a given category compared to all genes expressed in MTG. §Fisher's exact test of whether hDEGs near HARs/hCONDELs are enriched for a given category compared to all hDEGs. **(C)** Schematic highlighting SynGO terms that are enriched for hDEGs near HARs or hCONDELs in red. These enriched SynGO terms are concentrated at the synapse.

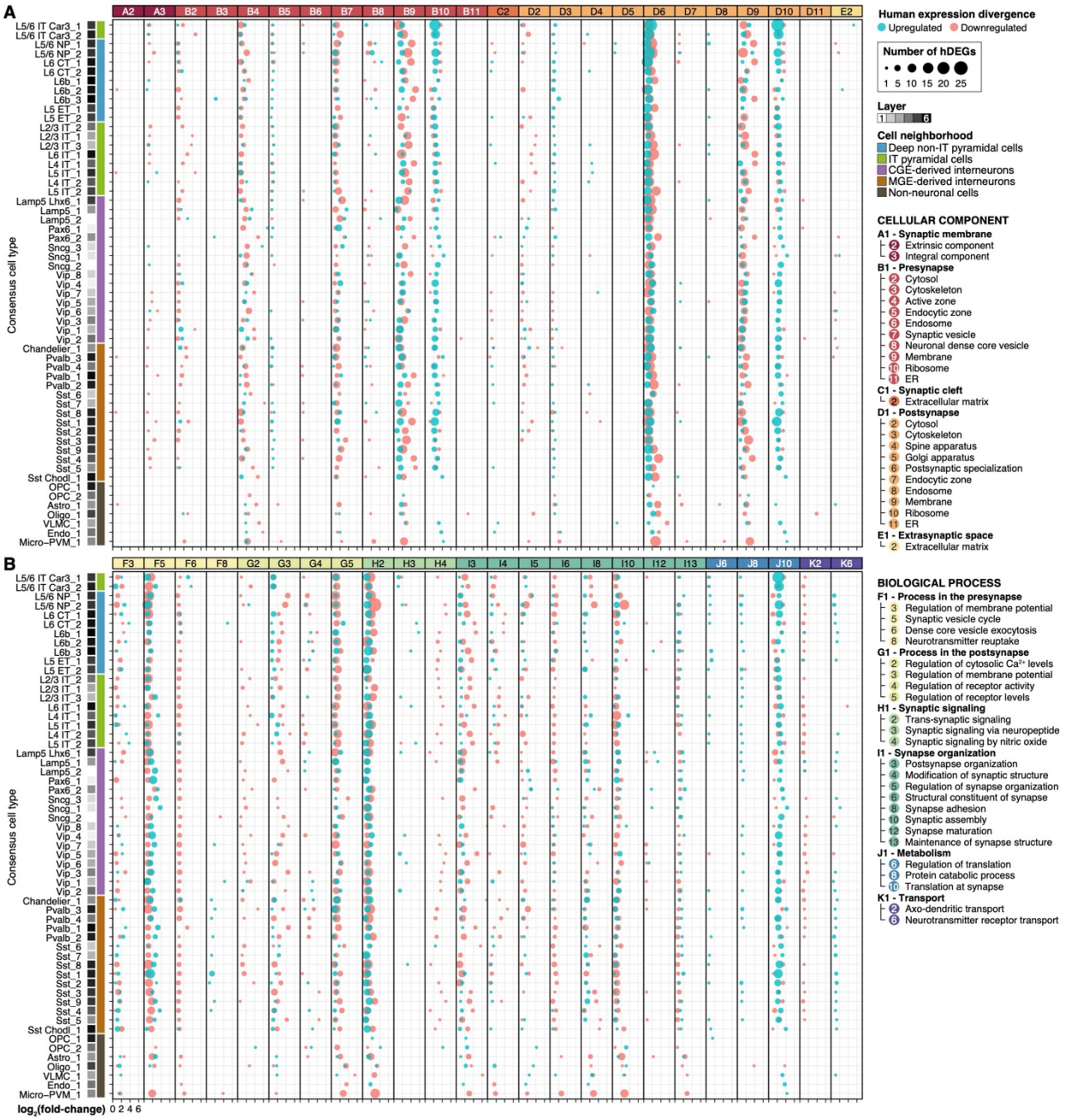

Fig. S19.

Analysis of human gene expression divergence of synaptic compartments and processes across consensus cell types. Dot plots showing the number of hDEGs in SynGO terms within Cellular Component **(A)** and Biological Process **(B)** categories across consensus cell types. Blue dots represent up-regulated genes, while red dots represent down-regulated genes. Dot sizes indicate the number of hDEGs per consensus cell type and SynGO term.

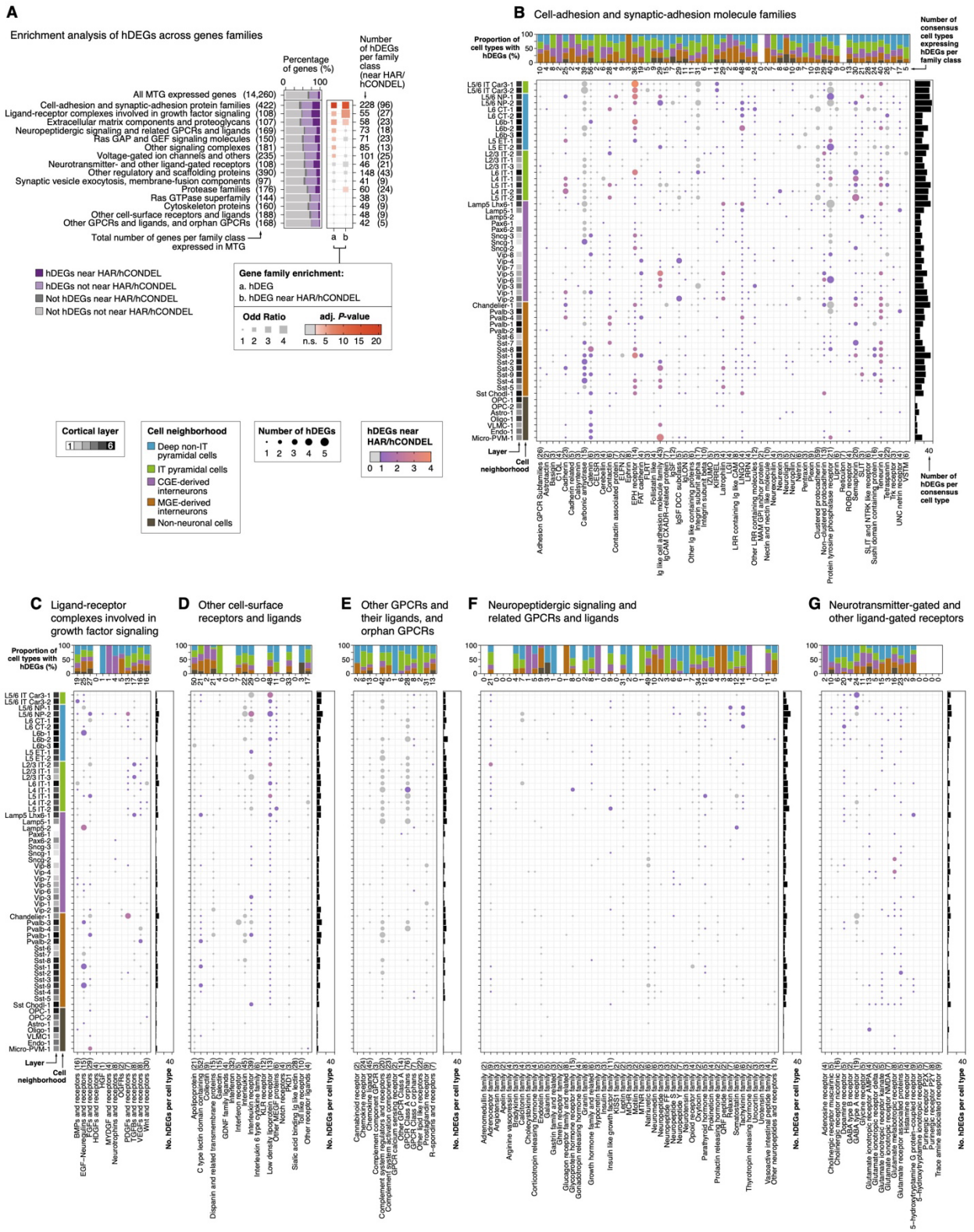

Fig. S20.
Expanded summary of hDEG enrichment near HARs or hCONDELs in gene families. (A) The proportion of genes that are hDEGs in at least one consensus cell type and/or are near HARs

or hCONDELs is plotted for all genes expressed in the MTG and manually-curated lists of gene families aggregated by their likely functional roles at the synapse (**Table S8**). [a]Fisher's exact test of whether hDEGs are enriched for a given category compared to all genes expressed in MTG. [b]Fisher's exact test of whether hDEGs near HARs/hCONDELs are enriched for a given category compared to all hDEGs. Heatmap colors indicate the significance of category enrichment; gray colors indicate non-significant categories. **(B-G, and continued in Fig. S21)** The number of hDEGs, the number of hDEGs near HARs/hCONDELs, and consensus cell type information is plotted for individual gene families for each category of gene families in (A).

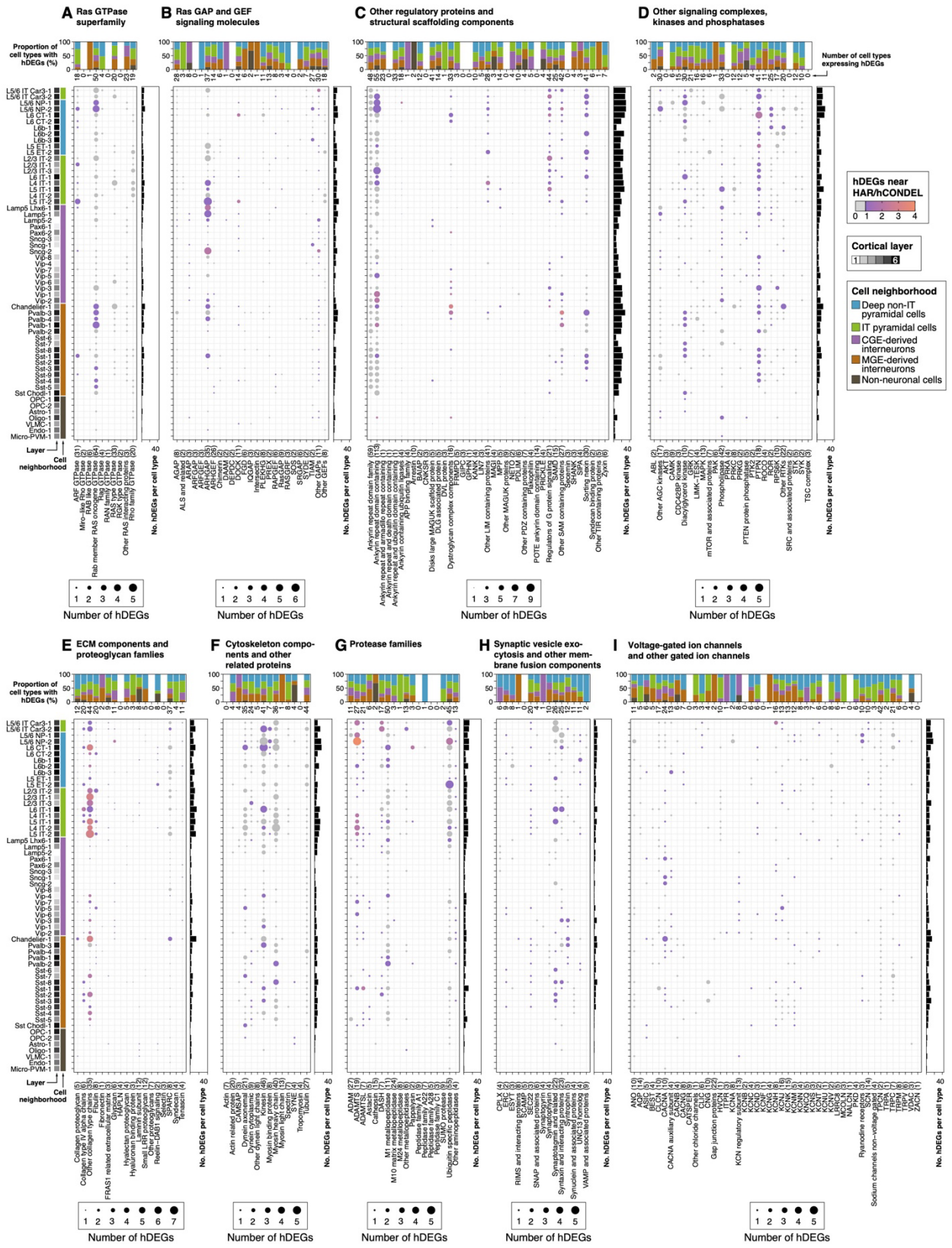

Fig. S21.
Expanded summary of hDEG enrichment near HARs or hCONDELs in gene families

(continued). Continuation of **Fig. S20**. The number of hDEGs, the number of hDEGs near HARs/hCONDELs, and consensus cell type information is plotted for individual gene families for each category of gene families in **Fig. S20A**.

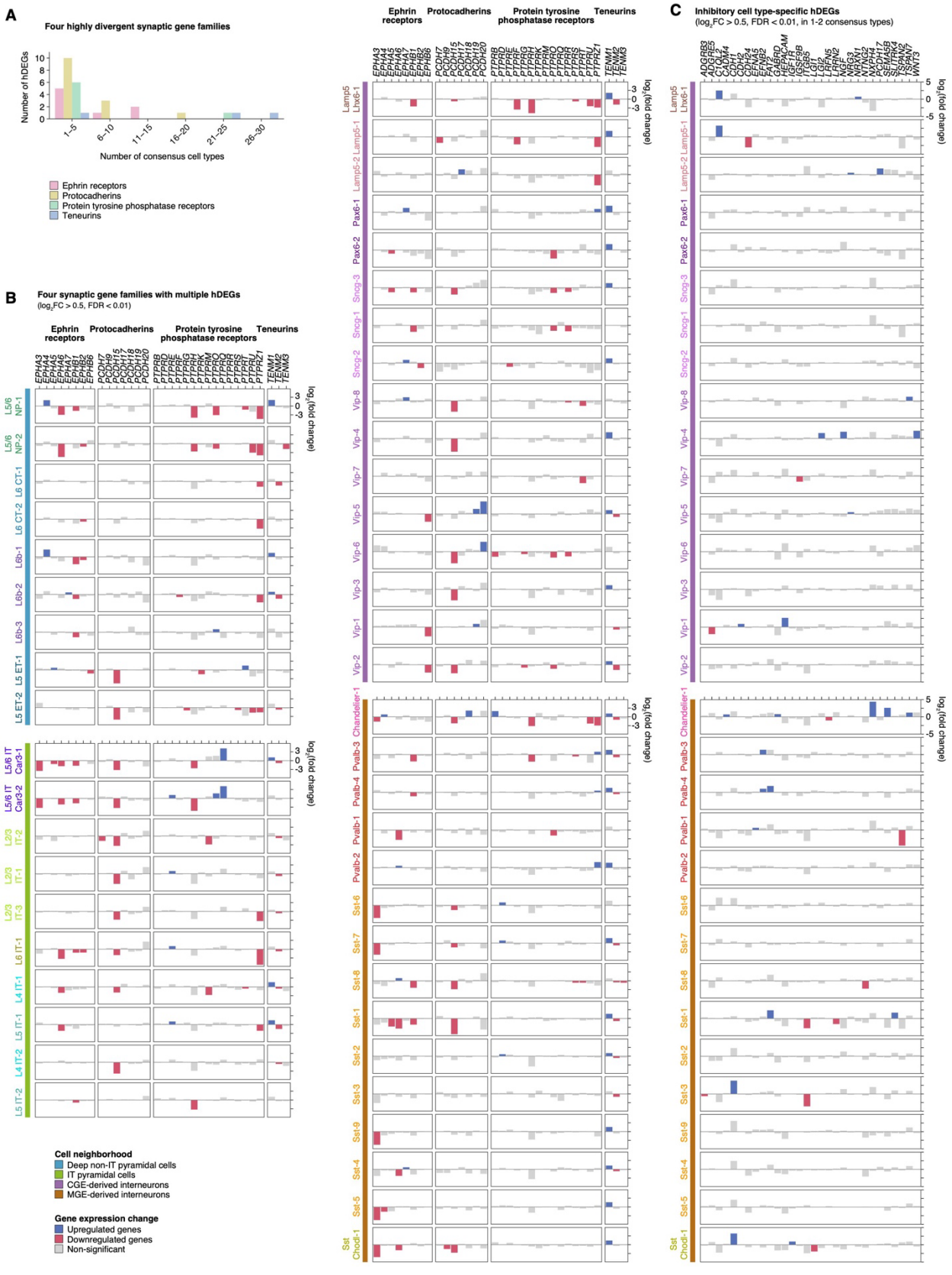
A
Four highly divergent synaptic gene families
Number of hDEGs
Number of consensus cell types
Ephrin receptors
Protocadherins
Protein tyrosine phosphatase receptors
Teneurins
B
Four synaptic gene families with multiple hDEGs
(log2FC > 0.5, FDR < 0.01)
Ephrin receptors
Protocadherins
Protein tyrosine phosphatase receptors
Teneurins
log2(fold change)
Cell neighborhood
Deep non-IT pyramidal cells
IT pyramidal cells
CGE-derived interneurons
MGE-derived interneurons
Gene expression change
Upregulated genes
Downregulated genes
Non-significant
C
Inhibitory cell type-specific hDEGs
(log2FC > 0.5, FDR < 0.01, in 1-2 consensus types)

Fig. S22.
Cell type specificity of human divergent synaptic gene programs. (A) Number of hDEGs across consensus cell types for four synaptic families that show high degree of divergence in cortical neurons from humans compared to non-human primates. Note that while a few genes (e.g. *TENM2*) are hDEGs in >25 consensus cell types, most members of these families show selective gene expression changes (in 1-5 consensus cell types). **(B)** Gene expression change of members of four highly divergent gene families in human excitatory and inhibitory neuronal types. Y-axis shows scaled fold change of expression in humans relative to non-human primates. Blue indicates human upregulated expression, red indicates human downregulated expression, and grey indicates no significant change in gene expression. **(C)** Examples of synaptic molecules that show gene expression changes specifically in 1-2 inhibitory consensus cell types.

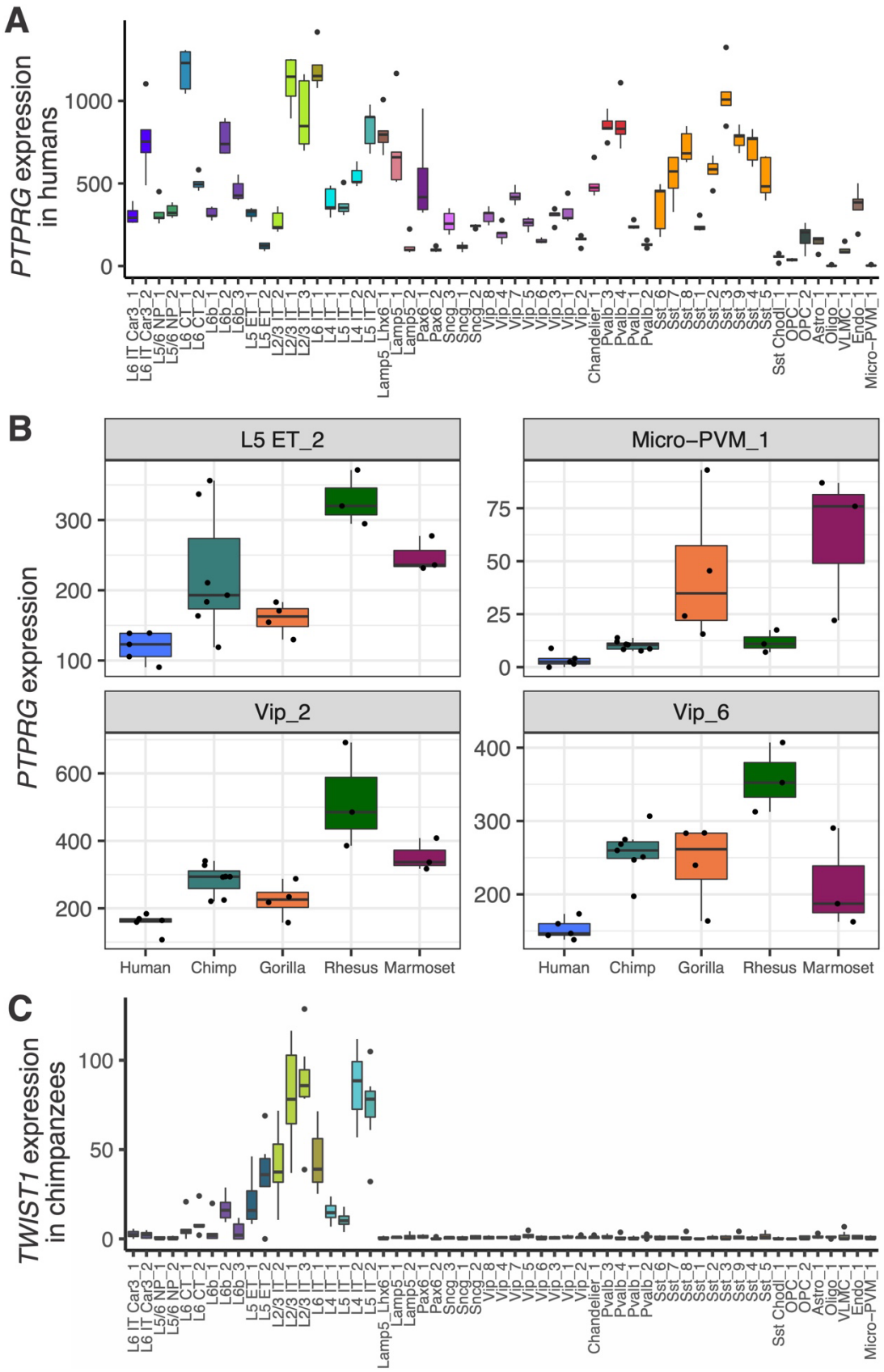
A
PTPRG expression in humans
1000
500
0
L6 IT Car3_1
L6 IT Car3_2
L5/6 NP_1
L5/6 NP_2
L6 CT_1
L6 CT_2
L6b_1
L6b_2
L6b_3
L5 ET_1
L5 ET_2
L2/3 IT_2
L2/3 IT_3
L2/3 IT_1
L6 IT_1
L4 IT_1
L5 IT_1
L4 IT_2
L5 IT_2
Lamp5_Lhx6_1
Lamp5_1
Lamp5_2
Pax6_1
Pax6_2
Sncg_3
Sncg_1
Sncg_2
Vip_8
Vip_4
Vip_7
Vip_5
Vip_6
Vip_3
Vip_1
Vip_2
Chandelier_1
Pvalb_3
Pvalb_4
Pvalb_1
Pvalb_2
Sst_6
Sst_7
Sst_8
Sst_1
Sst_2
Sst_3
Sst_9
Sst_4
Sst_5
Sst Chodl_1
OPC_1
OPC_2
Astro_1
Oligo_1
VLMC_1
Endo_1
Micro–PVM_1
B
PTPRG expression
L5 ET_2
Micro–PVM_1
Vip_2
Vip_6
300
200
100
75
50
25
0
600
400
200
400
300
200
Human
Chimp
Gorilla
Rhesus
Marmoset
C
TWIST1 expression in chimpanzees
100
50
0

Fig. S23.
***PTPRG* and *TWIST1* expression across consensus types and species. (A)** *PTPRG* expression in each consensus type in humans. **(B)** *PTPRG* expression is decreased in humans compared to NHPs in the consensus types L5 ET_2, Micro-PVM_1, Vip_2, and Vip_6. Points represent normalized *PTPRG* expression per individual. **(C)** *TWIST1* expression in each consensus type in chimpanzees.

Table S1.
Within-species cluster proportions across SMARTseq cortical layer dissections. Estimates of laminar distributions of clusters in human, chimpanzee, and gorilla based on the relative proportions of nuclei dissected from individual cortical layers.

Table S2.
Within-species subclass marker genes. Prior to DEG analysis, datasets were downsampled to a maximum of 100 nuclei per individual per cluster (finer curation resolution than subclass) in the Cv3 only samples. DEG analysis was performed on log-normalized gene expression matrices. The gene list was generated by implementing Seurat's FindAllMarkers function using the Wilcoxon sum rank test on a maximum of 500 nuclei per group (subclass versus all other cell types) within each species. Genes with Bonferroni adjusted p-values less than 0.05 were retained. This list is not filtered for orthologous genes and reflects the species-specific gene symbol.

Table S3.
Subclass differential gene expression across great apes. Gene list of pairwise differential expression comparing human, chimpanzee, and gorilla for each subclass. The gene list was generated by implementing a pseudobulk approach across individuals with DESeq2 using Ward's test on downsampled datasets with a maximum 50 nuclei per cluster per individual per species for Cv3 nuclei using one-to-one orthologous genes. Genes with Bonferroni adjusted p-values less than 0.05 were retained.

Table S4.
Subclass isoform switching across great apes. Relative isoform abundances were compared between human, chimpanzee, and gorilla for one-to-one orthologous genes with at least moderate expression. Gene expression and isoform proportions are reported for two individuals from each species that had SSv4 data. The column 'Large_prop_change' indicates if one species expresses a larger proportion (> 0.7, > 3-fold change on average across individuals) of a transcript than the other species (proportion < 0.1).

Table S5.
SST consensus type markers across species. List of marker genes that are differentially expressed in each of 9 *SST*-expressing consensus types relative to the other types. Markers were independently generated for each species. The gene list was generated by implementing the Wilcoxon sum rank test with Seurat's FindAllMarkers function on downsampled datasets with a maximum 100 nuclei per cross-species cluster per individual for Cv3 nuclei.

Table S6.
Consensus type cluster membership. 86 cross-species clusters included clusters from two or more species and were merged to give a final set of 57 consensus types with homologous clusters from all 5 primates.

Table S7.
Consensus type species-specific expression. Gene list of differential gene expression comparing each species to the other four species for each consensus type. The gene list was generated by implementing a pseudobulk approach across individuals with DESeq2 using

Ward's test on downsampled datasets with a maximum 50 nuclei per cluster per individual per species for Cv3 nuclei using one-to-one orthologous genes. Genes with Bonferroni adjusted p-values less than 0.05 were retained.

Table S8.
Analysis of hDEGs near HARs or hCONDELs. Lists of hCONDEL coordinates, hDEGs in consensus types that are near HARs or hCONDELs, potential HAR-hDEG interactions from existing PLAC-Seq datasets, and manually curated synapse-related gene families. This table also includes statistics on the enrichment of hDEGs, and hDEGs near HARs or hCONDELs, for SynGO and for manually curated lists of synapse-related gene families.

Supplementary Media 1.

Galleries of the spatial distributions of human MTG cell types. A representative human MTG section indicating spatial locations of 151 cell types grouped by subclass. Upper left images of each subclass show all types within the subtype. Note that for the rare types PVALB_3, PVALB_8, and SST_4, a mapped cell did not occur within the example section or was obscured by other cells in the section. For these 3 types, the cell locations were approximated based on laminar positions in other sections. L1: Cortical Layer 1; L2: Cortical Layer 2; L3: Cortical Layer 3; L4: Cortical Layer 4; L5: Cortical Layer 5; L6: Cortical Layer 6; WM: White Matter.